2 7 MAR 2000

Fluid-Optic Interactions II

Final Report

AFOSR Grant F49620-97-1-0489

Period Covered:
1 June 1997 – 31 December 1999

Principal Investigator: Eric J. Jumper

Hessert Center for Aerospace Research
Department of Aerospace and Mechanical Engineering
University of Notre Dame
Notre Dame, Indiana, 46556, USA

(219) 631-7680
FAX: (219) 631-8355

Email: Eric.J.Jumper.1@nd.edu

March 22, 2000

DTIC QUALITY INSPECTED 1

DISTRIBUTION STATEMENT A
Approved for Public Release
Distribution Unlimited

20000418 118

REPORT DOCUMENTATION PAGE

AFRL-SR-BL-TR-00-

0098

Public reporting burden for this collection of information is estimated to average 1 hour per response, includi... athering and maintaining the data needed, and completing and reviewing the collection of information. Send com... ction of information, including suggestions for reducing this burden, to Washington Headquarters Services, Directora... y, Suite 1204, Arlington, VA 22202-4302, and to the Office of Management and Budget, Paperwork Reduction Project

1. AGENCY USE ONLY *(Leave blank)*	2. REPORT DATE	3. R...
	22/3/2000	FINAL TECH. RPT.: 1 Jun 97 - 31 Dec 99

4. TITLE AND SUBTITLE
(U) Fluid-Optic Interactions II

5. FUNDING NUMBERS
PE - 61102F
PR - 2308
SA - BS
G - F49620-97-1-0489

6. AUTHOR(S)
Eric J. Jumper

7. PERFORMING ORGANIZATION NAME(S) AND ADDRESS(ES)
Department of Aerospace and Mechanical Engineering
University of Notre Dame
Notre Dame, IN 46556

8. PERFORMING ORGANIZATION REPORT NUMBER

9. SPONSORING/MONITORING AGENCY NAME(S) AND ADDRESS(ES)
AFOSR/NA
801 N. Randolph Street
Arlington, VA 22203-1977

10. SPONSORING/MONITORING AGENCY REPORT NUMBER

11. SUPPLEMENTARY NOTES

12a. DISTRIBUTION AVAILABILITY STATEMENT
Approved for public release; distribution is unlimited

12b. DISTRIBUTION CODE

13. ABSTRACT *(Maximum 200 words)*

This report describes fluid-optic interaction research at the University of Notre Dame. When a laser beam propagates through a variable-index-of-refraction, turbulent fluid, its optical wavefront becomes aberrated, reducing associated optical system performance. For flight above 0.6 Mach, "compressibility effects" alone become important in aberrating wavefronts. Scaling optical wavefront data collected in ground-test facilities to realistic flight conditions requires an understanding of the compressibility mechanism that produces wavefront distortions. This mechanism was studied using an analytical/numerical model. Shear-layer flows of low convective Mach number can be considered weakly-compressible, which allowed their velocity fields to be approximated using a discrete vortex method. From these "known" velocity fields, the concomitant pressure and density fields were determined by iteratively solving the unsteady Euler equations. The results showed that unsteady pressure fluctuations present in shear layers had a dominant effect on the resulting density/index fields; this effect has historically been neglected. The computed index fields produced simulated schlieren images which closely resembled experimental schlierens. Optical wavefronts computed from the simulation reasonably matched the behavior of large-scale aberrations measured in a transonic wind tunnel at AEDC. The compressibility model was used to suggest and test relations for scaling optical wavefronts from one flow condition to another. A simple density ratio successfully scaled distortion variations with altitude when shear layer Mach numbers were held constant; an additional temperature ratio was required if the velocity difference was kept the same. The spatial and temporal frequencies of optical distortions produced by dissimilar-index, incompressible, mixing flows were found to logically scale, provided the beam's diameter was larger than the largest flow structures.

14. SUBJECT TERMS
Fluid-Optic Interactions, Aero-Optics, Adaptive Optics, Wavefront Sensing, Compressible Flows, Compressible Shear Layers, Shear Layers, Mixing Layers, Turbulence, Scaling

15. NUMBER OF PAGES
67

16. PRICE CODE

17. SECURITY CLASSIFICATION OF REPORT	18. SECURITY CLASSIFICATION OF THIS PAGE	19. SECURITY CLASSIFICATION OF ABSTRACT	20. LIMITATION OF ABSTRACT
Unclassified	Unclassified	Unclassified	UL

Executive Summary

This report covers the activities at the University of Notre Dame under AFOSR Grant F49620-97-1-0489, "Fluid-Optic Interactions II." The report begins with a discussion of the relevance of the research to Air Force missions and places the work in context with work performed prior to the time the grant effort was begun. When a laser beam propagates through a variable-index-of-refraction, turbulent fluid, its optical wavefront becomes aberrated, reducing associated optical system performance. At flight Mach numbers above ~ 0.6, "compressibility effects" alone become important in aberrating wavefronts. Scaling optical wavefront data collected in ground-test facilities to realistic flight conditions requires an understanding of how this compressibility mechanism produces wavefront distortions. Prior to this grant's research, little was known about this compressibility mechanism. This compressibility mechanism was studied using an analytical/numerical model. Because the shear-layer flows in question have low convective Mach numbers, they can be considered weakly-compressible, which allows their velocity fields to be approximated using a discrete vortex method. From these "known" velocity fields, the concomitant pressure and density fields were determined by iteratively solving the unsteady Euler equations. The results showed that unsteady pressure fluctuations present in shear layers had a dominant effect on the resulting density/index fields; this effect has historically been neglected. The computed index fields produced simulated schlieren images which closely resembled experimental schlierens. Optical wavefronts computed from the simulation reasonably matched the behavior of large-scale aberrations measured in a transonic wind tunnel at AEDC. An explanation for small-scale distortions observed in these experimental data was formulated, suggesting that temperature discontinuities in the splitter-plate boundary layer had been fed into the shear layer. The compressibility model was used to suggest and test relations for scaling optical wavefronts from one flow condition to another. A simple density ratio successfully scaled distortion variations with altitude when shear layer Mach numbers were held constant; an additional temperature ratio was required if the velocity difference was kept the same. Optical distortions produced by dissimilar-index, incompressible, mixing flows were found to have a different character than those from weakly-compressible flows; however, the spatial and temporal frequencies of low-speed distortions were found to logically scale, provided the beam's diameter was larger than the largest flow structures. The results of the research were communicated directly to DoD personnel working in the technical area as well as being presented at several national technical meetings. The work is documented in a Ph.D. Dissertation, six meeting papers, and four journal articles.

Contents

Final Report

FLUID-OPTIC INTERACTIONS II

AFOSR Grant F49620-97-1-0489

Principal Investigator: Eric J. Jumper

Hessert Center for Aerospace Research

University of Notre Dame

Notre Dame, Indiana, 46556, USA

(219) 631-7680

FAX: (219) 631-8355

Email: Eric.J.Jumper.1@nd.edu

1. INTRODUCTION

The use of optical signals propagated through fluids is ubiquitous in Air Force and DoD applications. These applications include, but are not limited to, imaging distant objects from ground-based and airborne systems, tracking, communication, ranging, sensing incoming threats, irradiating targets for weapons-delivery identification, and destroying targets by irradiation with high-power lasers. These latter systems include airborne laser weapons such as the Air Force's Airborne Laser (ABL) theater ballistic defense system.

Aberrations (distortions of figure) on optical wavefronts degrade the ability of an optical system to image, focus, or otherwise use the optical signal associated with the propagating wavefront for the system's intended purpose. When an otherwise-planar (flat-figured) wavefront propagates through an optically-active field (i.e., a field of variable index of refraction), the wavefront emerges aberrated. If the imposed aberrations are known and constant, measures may be taken to compensate

for the aberrations to improve the performance of the optical system; however, when the aberrating field is rapidly time-varying, the problem of compensation becomes more complicated. In the case of a fluid-optic interaction, the distortion is caused by a dynamically-changing turbulent flowfield; thus, the wavefront's aberrations themselves are also dynamically changing. Although the spatial and temporal frequencies of the optical aberrations are related to the spatial and temporal character of the turbulent flowfield, the optical aberrations result from an integrated path through the variant-index field associated with, but not identical to, the turbulent flowfield. As such, optical aberrations cannot be directly related to any particular instantaneous spatial feature in the flowfield; however, the fact that the aberrations are associated with features in the turbulent flowfield, features which convect at some velocity in the flow direction, means that the aberrated features on the wavefront also "convect" in the flow direction. This fact has been of critical importance to our research.

1.1. Defining the Fluid-Optic Interaction Problem

This system-performance reduction induced by turbulent, variant-index flowfields can be quantified by analysis of the far-field irradiance pattern.[1] Light transmission through such time-varying, aberrating fields can occur over short path lengths in the "near field" (i.e., path length, y, on the order of the system aperture diameter, A), or can occur over extended paths (i.e., path lengths, y, much larger than A). It should be noted that the term "near field" in the present context refers to aberrating fluid structures very near the exit aperture of an outgoing collimated beam, or at the receiving aperture for an imaging system. This should not be confused with the "near field" in physical optics, where the Fresnel approximations, but not Fraunhofer approximations can be applied. The former, short-path (near-field) aberration is usually termed "aero-optics" and the latter, long-path aberrations are usually termed "atmospheric propagation." These classifications have their origin in the specific ap-

plications with which they are associated (see Refs. 2 and 3, for example). It has long been known that placing a conjugate waveform on the beam prior to its transmission through the aberrating medium (or prior to focusing for a system receiving an optical signal that has traversed the aberrating medium) results in the emergence of a planar-wavefront beam as it leaves the medium (or enters a focusing mechanism after traversing the medium); systems that sense the aberration, construct and apply the proper conjugate waveform at regular time intervals are termed "adaptive-optic systems," and the study of such systems is known as "adaptive optics."[4] The determination of the design requirements for such systems depend on understanding the spatial and temporal frequencies of the distorted optical wavefront for the applicable aberrating flowfield.

Over the last decade, progress has been made in both measuring the wavefront dynamics for the atmospheric propagation problem and using this information for designing and applying adaptive-optic equipment and techniques.[5] For aero-optic problems, on the other hand, progress in adaptive-optic correction has been essentially nonexistent. The reason for this is that the required spatial and temporal frequencies associated with aero-optic problems are at least an order of magnitude greater than those presently correctable by adaptive-optic systems for the atmospheric-propagation case, even for relatively-slow laboratory flows.[5,6] As such, the main research thrust in aero-optics until very recently has been to attempt to quantify the time-averaged, statistical, near-field wavefront distortion (as phase variance or *root-mean-square* Optical Path Difference, OPD_{rms}) in order to estimate the time-averaged, far-field degradation that might be expected for a system whose optical signals must traverse the aberrating, turbulent flowfield.[7] In this context, "far field" is defined as the region where the diffraction integral can be determined using Fourier Optics.

It is helpful in understanding fluid-optic interaction problems to divide the

problems into four levels of understanding associated with either the atmospheric propagation problem or the aero-optic problem. These levels may be generally arranged in their order of complexity as follows: first, there is the level of understanding that allows one to estimate the statistical level of optical distortion that is likely to be encountered for a particular optical propagation scenario through a flowfield. At the second level, one can predict not only the statistically-averaged distortion but also the spatial and temporal frequencies associated with the time-varying optical distortion. The third level is reached when actual time histories associated with the optical distortions can be measured and linked to the specific fluid-mechanic character of the flowfield. With a fourth-level understanding, the optical distortions can be measured rapidly enough to allow adaptive-optic compensatation for the distortions, thereby improving/restoring the optimal performance of the optical system. The atmospheric propagation problem has advanced through all four levels of understanding, while until the span of time that covers our initial AFOSR funding, the aero-optic problem remained at level one, and the researchers in the field had no prospects or apparent aspirations to move to a higher-level understanding. A historical review of aero-optics is given as APPENDIX A that attempts to place the statistical approach in perspective. The review includes reference to Refs. 8–9 that span the period from 1952[8] to 1992.[9] Our first grant (F49620-93-1-0163) began one year later in 1993.

1.2. Association of Aero-Optics with Fluid Mechanics.

It is clear from APPENDIX A that the aero-optic problem has always been inextricably linked with the fluid mechanics of turbulent flows. This is in contrast to the atmospheric-propagation problem which has been treated almost exclusively as an optical problem. For astronomical observations, assuming that viewing conditions are favorable, the aberrating structures are large compared to the viewing aperture. Often these structures are of such extent that the aberrations can be treated as sim-

ple tilt corrections,[5] and smaller aberrations are still relatively large with respect to the aperture, so that only the first few aberration modes need be addressed in order to restore much of the aberration-degraded system performance. These facts mean that the resolution of a wavefront sensor to detect the aberrations need not be exceptionally high. Beyond this, the aberrations "convect" through the viewing aperture at speeds associated with atmospheric winds plus any slue rates that may be superimposed. Typical rates required to provide time-resolved measurements of the aberrated wavefronts due to propagation through the atmosphere are on the order of hundreds of Hertz. Wavefront sensor technology has for some time been capable of achieving these rates.[4,5]

The aero-optic problem, by its very nature, must contend with shear-layer and boundary-layer aberrations whose sizes are on the order of the associated turbulent structures; further, the convection rates are now associated with the defining flows which can be much higher than typical atmospheric winds (in the case of flow over an aircraft in flight, for example). Our efforts have shown that even for a laboratory flow of less than 10 m/s, because of the small size of the turbulent structures, wavefront capture rates of 5 kHz are needed to time-resolve the dynamics of the aero-optic wavefront aberrations. Until very recently, the fastest wavefront sensors available operated at less than 1 kHz (see discussion of Shack-Hartmann Sensors in APPENDIX B). For this reason, equations linking the statistical, optical-aberration field over the aperture, like Eq. 12 in APPENDIX A, were developed. Examination of Eq. 12 shows that this estimate depends entirely on statistical measures of the fluid-mechanic properties of the turbulent flowfield over the viewing aperture.

1.3. The Aero-Optic, Adaptive-Optic Problem

As mentioned above, in order to even scope the order of complexity associated with attempting to provide an adaptive-optic correction for optical propagation through

an aero-optic field, a level-two understanding of the aberrations is needed. In 1992, practitioners in the field of aero-optics felt that, with no hope of a significant breakthrough in wavefront sensor technology, the field of aero-optics could never mature to the level of addressing adaptive-optics; however, some few of us were at least curious about the requirements of an adaptive optic system for the aero-optics problem. My early attempts at determining estimates for the spatial and temporal frequencies relevant to the aero-optics problem using the statistical measures of turbulence were less than satisfactory, and served as the basis for our first AFOSR grant. That grant initially sought only to address this question; i.e., it sought to obtain a level two understanding of the aero-optic problem. Work performed in the late 1980's, had suggested to us that there might be a way of measuring these spatial and temporal frequencies. In Refs. 10 and 11, Malley *et al.* describe a simple optical device that, when coupled with certain fluid-mechanic principles, was capable of directly measuring the statistical OPD_{rms}. APPENDIX B describes the principles associated with the instrument, along with some background on Hartmann wavefront sensors.[12]

In that first round of funding, we soon came to realize that the fundamental assertion upon which the Malley *et al.* instrument was based had the potential of developing an actual wavefront sensor. One major accomplishment of the first grant was the development of the SABT (Small-Aperture-Beam Technique) wavefront sensor.[6,13] The (one-dimensional) SABT sensor is described in APPENDIX C. In this round of funding, a two-dimensional version of the sensor was developed as described below.[14,15] The SABT sensor made possible for the first time the ability to examine the time-resolved dynamics of the aero-optically aberrated wavefront. We studied wavefronts distorted by propagation through turbulent shear flows between fluids of dissimilar index of refraction; in particular, we extensively studied propagation through the transitional region of a heated, two-dimensional jet. Fig. 1, produced

using a numerically-simulated flowfield,[13] is helpful in understanding the nature of the optical aberrations produced by propagation through the heated jet. At an instant in time, an initially-planar wavefront propagates through the aberrating flowfield, also shown at that instant, and emerges with the distorted wavefront shown. In this case, the aberration is due to the mixing of dissimilar index-of-refraction flows. Although the distortion is due to a path integration through the flow, it is possible to associate features on the wavefront with flow features. As the flowfield convects and evolves, a footprint of the character of the evolving flowfield is captured by the wavefront; a time series of the instantaneous wavefronts, as shown at the upper portion of Fig. 1, captures the dynamics of the shear layers of the two-dimensional jet. The characteristic hills and valleys, and the slopes of these features with time, indicate the convective and evolving nature of the flowfield; different structures convect at different rates as evidenced by the different slopes of the hills and valleys. The fact that the shear-layer roll up is organized can be seen by the well-ordered nature of the time series of wavefronts.

An actual time series of experimentally measured wavefronts from the heated-jet experiments is shown in Fig. 2.[6] It is clear that the features found in the simulated field are present in the experiments. Time series of the Fig. 2 type were studied in order to assess the adaptive-optic correction requirements that would be needed to improve/restore the Strehl ratio, a measure of performance (see APPENDIX A, Eq. 13). Fig. 3 gives a collage of representative results from Ref. 16; the equation defining the Strehl Ratio, SR, is given in the lower left corner of the figure. The upper-right corner of Fig. 3 shows the far-field focus for a periodic application of a perfect correction restoring the Strehl ratio to 1.0 each time it is applied. In between these applications, the focus degrades as the aberration changes with the convecting and evolving turbulent structures. In this particular example, the uncorrected, time-averaged Strehl

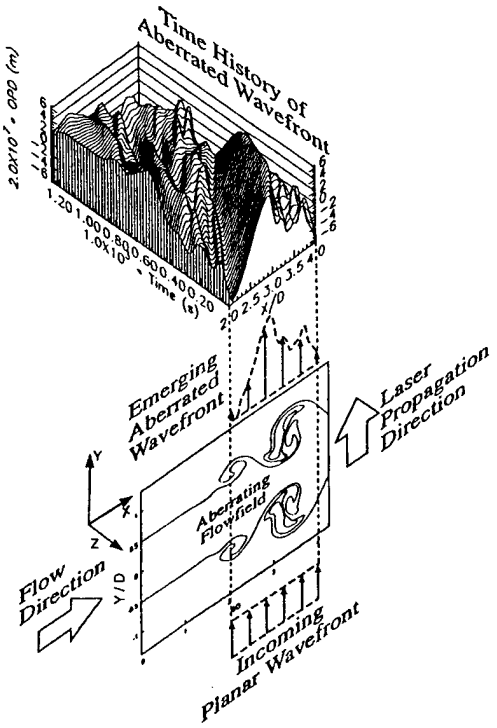

Figure 1. Schematic of a planar wavefront propagating through a two-dimensional heated jet and concomitant time series of one-dimensional, aberrated wavefronts.

ratio was 0.265; i.e., the peak intensity of the focal point was approximately 26% of a diffraction-limited peak intensity. For this example, propagation through a 7 m/s jet, a perfect correction would have to be applied at 10 kHz to restore the Strehl to greater than 95% diffraction-limited intensity. With a four-by-four-element deformable mirror over the aperture shown, also cued at 10 kHz, the Strehl ratio would be restored to approximately 75% of diffraction-limited. The lower-right figure indicates that the restoration will be further reduced if the correction applied is itself "late." This means that in order to maximize the restored intensity the applied correction must be correct at the time it is applied.

Most future aero-optic research will be done in ground-test facilities. The difficulties of testing in compressible-flow facilities (cost, test-section size, test duration,

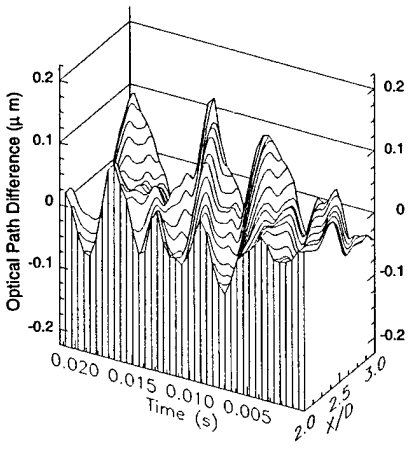

Figure 2. Space-time representation of SABT-measured OPDs for propagation through an experimental, two-dimensional, heated jet flowfield (from Ref. 6).

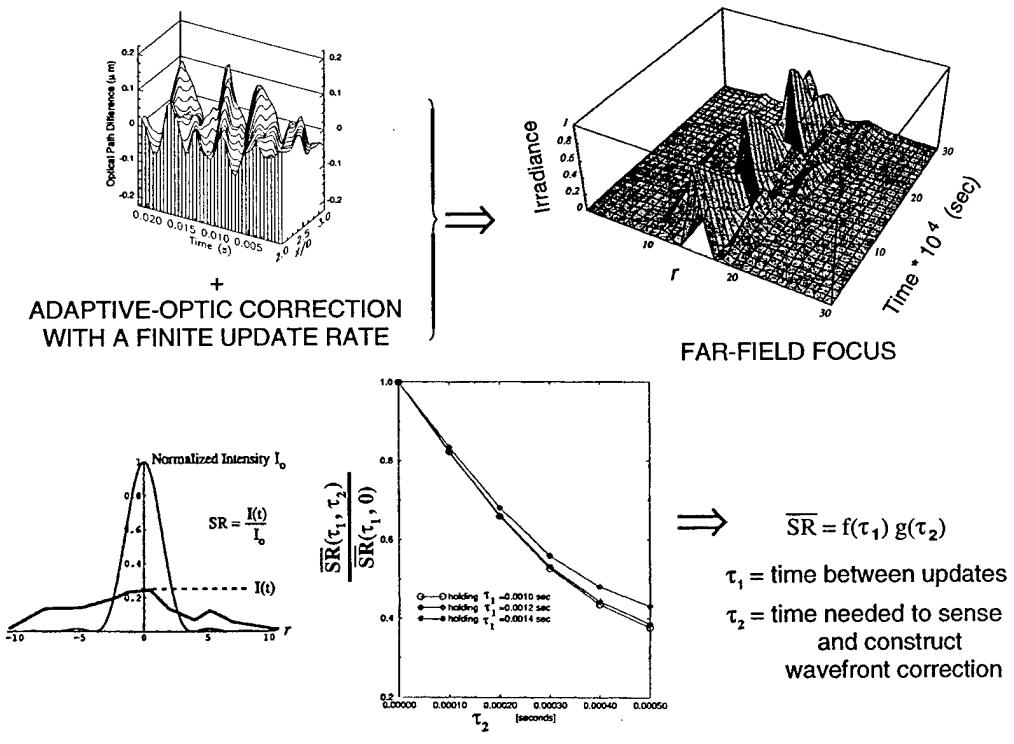

Figure 3. Adaptive-optic correction requirements study.

vibration) will limit the number and success of such tests; in many instances, aero-optical distortions have been and will continue to be produced by low-speed ($\sim$ 7 m/s, say) mixing of dissimilar-index, incompressible flows. The presumption inherent in using low-speed flows for aero-optic research is that the results of such research will also be applicable to high-speed aero-optics. The question, then, is how would wavefront data collected in ground-test facilities scale to other flight conditions and, in particular, can data obtained in low-speed flows be used to infer distortions created by high-speed flows?

In the last stages of our first funding round, we used the SABT sensor to measure the wavefront dynamics of propagation through the Mach 0.8 compressible shear layer at the Arnold Engineering Development Center (AEDC).[17,18] Fig. 4 shows an example time series of experimental wavefronts from these tests; these data were taken at station 2, roughly one half meter downstream from the splitter plate. It is clear from the figure that the dynamics of the wavefront aberrations are indeed similar in character to those for propagation through the heated jet (compare Fig. 4 to Fig. 2, for example). For the wavefront structures shown in Fig. 4, when compared to those in Fig. 2, the sizes of the AEDC structures (i.e., spatial scale) are roughly eight times larger than those wavefront structures for the heated jet. At the same time, the convection velocity of the structures in the AEDC experiments increased by roughly forty times. Thus, one might conclude that for an adaptive-optic system to perform at the same level of restoration as for the heated jet, using a similar number of subapertures, would require corrections to be made at 60 kHz; however, our initial attempts at scaling heated-jet OPD structure sizes/frequencies to predict the AEDC measurements was unsuccessful, casting doubt on how adaptive-optics requirements would scale for other system apertures and conditions. This is not just an academic exercise. A large-scale weapon system with $\sim$ 1-m aperture is being

prepared for fielding (i.e., the ABL); yet, there was no method for estimating aero-optical effects the system might expect prior to the presentation of some of this grant's research at the Second Annual Directed Energy Symposium (1–5 November 1999).[19,20] Thus, scaling issues were the focus of a large portion of the work of this round of funding (F49620-97-0489). The individual objectives of the present grant's research are discussed in the next section.

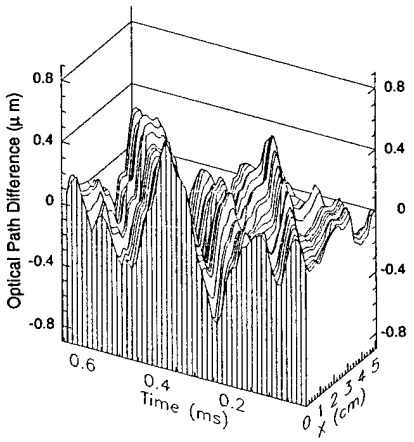

Figure 4. AEDC station 2 SABT-measured wavefronts: beam separation = 2.5 cm, High-Pass Filter = 2500 Hz. (From Ref. 18.)

2. OBJECTIVES OF THE RESEARCH

The primary objective of the present grant's research was to address the scaling issues that came to light in studying the similarities between optical aberrations due to propagation through the heated jet and propagation through the compressible shear layer. Additional objectives were to: (a) extend some of the instrumentation-development work of the last grant by developing a derivative, two-dimensional wavefront sensor of the one-dimensional Small-Aperture Beam Technique (SABT) sensor; (b) investigate the possible use of control to develop a scheme for real-time sensing and correcting the wavefront for propagation through compressible shear layers; and (c) further explore

the relationship between the wavefront aberrations and the concomitant aberrating structures. The approach and results for the scaling objective are described in Section 3. The approaches and results for the remaining objectives are described in Sections 4–6.

3. SCALING OF OPTICAL ABERRATIONS

3.1. Approach

To develop reliable scaling relations requires a basic understanding of the phenomenon to be scaled (in this case, compressibility-caused, optical aberrations). Prior to this grant, we tried scaling the spatial and temporal frequencies of distortions created by a low-speed, heated jet using relations from the fluid-mechanics literature, but we could not match the frequencies measured in a compressible shear layer using the SABT sensor.[21] Without a fundamental understanding of the compressibility mechanism, the reasons for this difficulty were not understood.

The mechanism by which light is aberrated by transmission through a shear layer composed of two, dissimilar-index fluids is fairly well understood.[22] Prior to the present grant's research, the same could not be said for a shear layer where the index-of-refraction variations are due to compressibility. Cassady's[23] Navier-Stokes simulation, for instance, only modeled aero-optical distortions produced by the dynamics of shear-layer reattachment, not those caused by shear layer coherent structures. Direct numerical simulations of compressible shear layers had been performed by the early 1990's,[24,25] but these studies were primarily interested in shear-layer stability and the resulting coherent structure shapes rather than on the instantaneous density fields required for aero-optical calculations. As late as 1998, some researchers were implicitly assuming the compressibility mechanism to be the same as that for dissimilar-index mixing; for example, Dimotakis *et al.*[26] measured optical distortions produced by

a compressible mixing layer using streams of markedly different index-of-refraction, thereby overwhelming any aberrations created by compressibility alone. The lack of compressibility-mechanism understanding became apparent to us when the first compressibility model attempted during the present research was explained to a group of experts in compressible shear layers and in aero-optics at a 1998 technical meeting. While all in attendance agreed that this initial model produced unrealistically-low aberrations, no one was sure what was missing from the model.[27–29]

Thus, the primary goal of the research under this grant was to delve into this question of the compressibility mechanism and, based on those results, suggest how ground (or flight) test data might be scaled. As such, this research, in effect, constitutes an enabling technology required for future success in adaptive-optic correction of aero-optic distortions.

The present research began with two things that could be exploited from our first grant (F49620-93-0163). The first of these was the database of optical wavefront measurements serendipitously obtained in a compressible shear layer. Although some of this data had already been reported in the literature,[17,18] much of the database had not been examined prior to the present grant. This wavefront data was used to anchor the analytical/numerical model developed during the present research.

The second item that was used was Hugo's numerical shear-layer simulation.[22] Hugo developed the simulation as a tool for testing algorithms required in the development of the SABT wavefront sensor. For his purposes, the simulation only needed to provide a deterministic, index-of-refraction field that evolved as it convected downstream.[22] The present study, however, further required that the simulation compute a realistic, first-order estimate of the time-varying velocity field produced by a weakly-compressible shear layer. These velocity fields provided a common base flow for further analysis and allowed direct comparison of the index fields and resulting aero-

optic distortions produced by both incompressible and weakly-compressible flows.

Analytical/numerical methods were then used to determine index-of-refraction (or equivalently, density) fluctuations in a weakly-compressible shear flow. A compressibility model was developed in which a series of mechanisms were overlaid on the common velocity field to compute the time-varying density field. Optical wavefronts were then computed by (numerically) propagating an optical beam through the time-varying index (density) field. The validity of the overlaid mechanisms was assessed by comparing the character of the computed aero-optical distortions to those measured experimentally in the similar, weakly-compressible, shear layer discussed above.[18] The experimentally-anchored compressibility model was then accepted as the basis for developing appropriate relations for scaling aero-optic distortions to other conditions (e.g., ground test to flight).

3.2. Re-reduction of AEDC Experimental Data

The AEDC optical wavefront data, first presented and examined in Refs. 17 and 18, documented the optical distortions created by a compressible shear layer over a limited, 5-cm, test aperture. The AEDC test section is shown schematically in Fig. 5. As discussed in Ref. 17, a post-test, high-pass digital filter was employed to remove signal noise caused by vibration of the test section's optical access windows. In this earlier work, the cutoff frequency was conservatively chosen in order to minimize the chances of vibrational corruption of the beam jitter data;[17] the 2–2.5-kHz corner frequency was also chosen because the small measurement aperture already functioned as a spatial filter for any larger-scale structures. For this data to be used to anchor the analytical/numerical models developed during this grant, a lower corner frequency was desired in order to retain the influences of flow structures larger than the test aperture, as explained below and documented in Refs. 30–32.

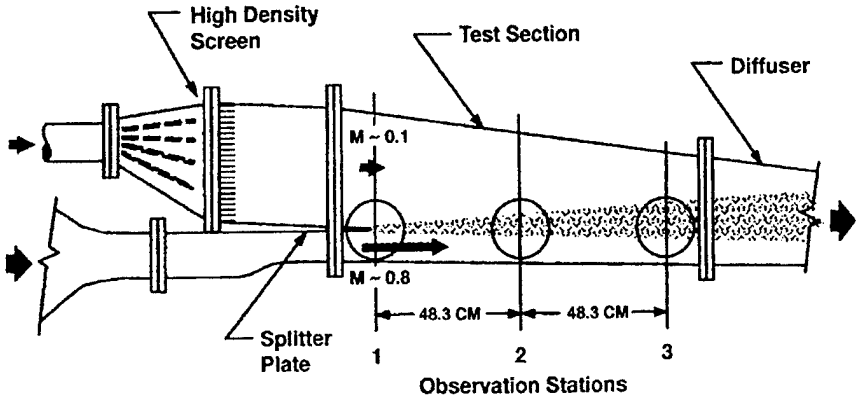

Figure 5. Schematic of AEDC facility (From Ref. 33).

The growth rate of a shear layer is now well understood to be driven by the growth of organized, coherent structures.[34,35] This growth rate has been characterized in semi-empirical laws for incompressible shear layers[36,37] with corrections for compressibility.[37–39] If the aberrating structure had a characteristic size, Λ, the wavefront's frequency of variation, $f_{\overline{OPL}}$, would be expected to vary with the structure's convection velocity U_c as

$$f_{\overline{OPL}} = \frac{U_c}{\Lambda}. \tag{1}$$

The average coherent structure (a vortex "roller") diameter, δ_{viz}, measured from schlieren photographs of compressible shear layers, can be estimated from the following empirical relation reported in the literature:[39]

$$\left(\frac{\delta_{viz}}{x}\right) = C_\delta \frac{(1 - r_u)(1 + \sqrt{s})}{1 + r_u\sqrt{s}}, \tag{2}$$

where r_u is the velocity ratio U_2/U_1, $s = \rho_2/\rho_1$ and C_δ is a constant. For the AEDC conditions, Eq. 2 predicts $\delta_{viz} \approx 12.6$ cm at the center of the station 2 aperture; that is, a structure more than twice the size of the 5-cm test apertures used for both the SABT and the holographic interferometry study for which the AEDC facility was originally designed.[33] The effect of the aperture is to act as a spatial filter on the measured wavefront. The distortion caused by these largest-scale flow structures is reduced to

a time-varying, tilt aberration with a period indicative of the large-scale structure.[23,40] The large-scale structures' size and convection velocity ($U_c \sim 150$ m/s)[39] would lead one to expect tilt-distortion variation frequencies of $f_{\overline{OPL}} \sim 1.2$ kHz, well below the corner frequency of the originally-used vibration filter. In the original study funded under our first grant (and documented by Ref. 18), no attempt was made to try to understand the relevant physical cause of the aberrations; Ref. 18 sought simply to present the aperture-restricted data. The present grant research, however, was specifically interested in understanding the underlying physics of compressibility and anchoring numerical simulations to these AEDC data. Thus the present research required a more careful selection of the high-pass corner frequency in order to remove the vibration corruption, on the one hand, but to preserve the largest-scale-structure influences on the other. A careful reexamination of the AEDC data showed that the filter's corner frequency could be safely reduced to 750 Hz (as described in Refs. 30–32).

With this lower vibration-removal filter setting, clear evidence of large-scale structures was present in AEDC station 2 OPD time-series data as shown in Fig. 6. These large-scale flow structures appear to be comparable in size to the rollers (vortices) created during shear-layer rollup. For optical systems with greater than 5-cm apertures, the structures would also produce much larger overall OPDs than originally reported. Since typical airborne telescopes and laser systems use apertures much larger than the 5-cm aperture tested at AEDC, significantly larger optical degradation than reported in Refs. 17 and 18 could result.

Distortions created by smaller-scale flow structures were present in the AEDC station 1 OPD data as shown in Fig. 7. Since this aperture began at the splitter-plate trailing edge, these smaller-scale structures were too large to be caused by shear-layer rollup. A possible mechanism was suggested to explain smaller-scale distortions

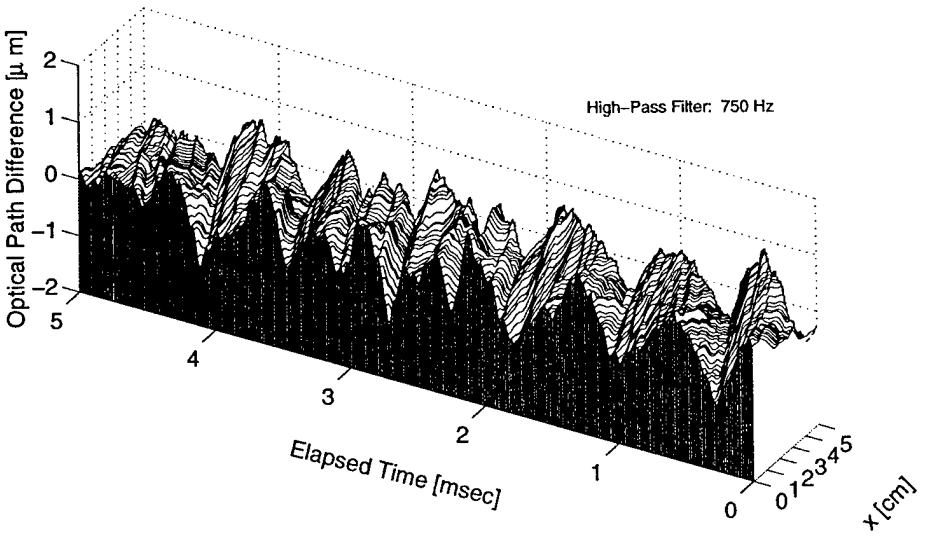

Figure 6. AEDC station 2 experimental wavefront reconstruction: beam separation $\delta = 2.54$ cm.

observed in both the station 1 and station 2 wavefronts. If this mechanism proves to be correct, the overall wavefront might be modeled as a superposition of large- and small-scale distortions (see below). The small-scale distortions might then be removable by, for example, boundary layer suction. This theory is described in more detail in Refs. 30–32.

3.3. Analytical/Numerical Model

To investigate the physical mechanisms which produce optical distortions in compressible shear layers, optical wavefronts were computed for a numerical flowfield model. The numerical simulation's velocity boundary conditions matched those of the AEDC testing described above. The simulation had two distinct parts: (1) a velocity field modeled using a discrete vortex method (DVM) and (2) an index-of-refraction model used to determine the corresponding density field (and index-of-refraction field) from the (input) velocity field.

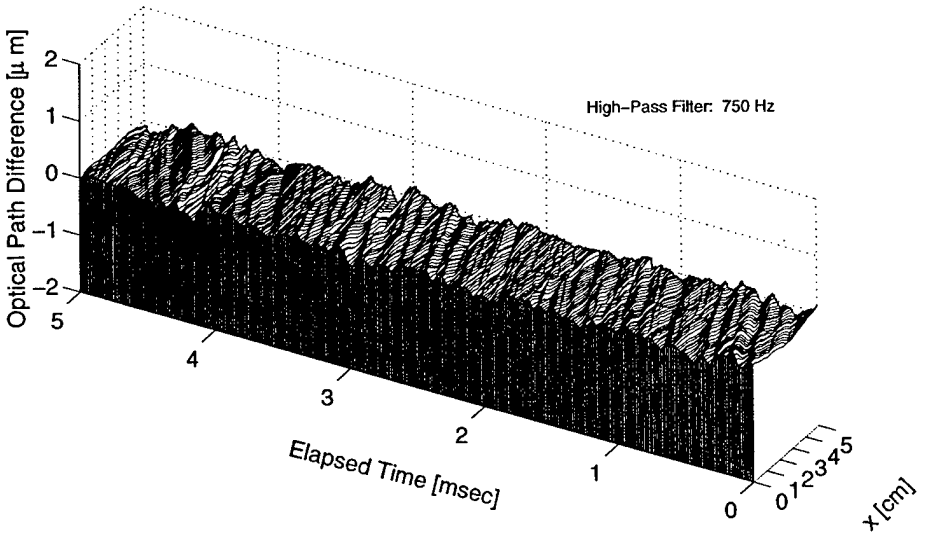

Figure 7. AEDC station 1 experimental wavefront reconstruction: beam separation $\delta = 2.54$ cm.

The initial, transitionally-turbulent flowfield in a shear layer is dominated by the shear-layer rollup caused by the inviscid Kelvin-Helmholtz instability mechanism.[41] This rollup has been successfully simulated using various inviscid and pseudo-inviscid methods.[42–45] The shear layer for the present study was modeled by modifying the discrete-vortex-method (DVM) code developed under our first grant. One of the primary advantages of using a DVM is that it is a reduced-order, pseudo-inviscid method. As such, the DVM is able to model a shear flow with a fairly small computational domain, thereby producing considerable computational savings. A second advantage is the simplicity of the DVM model itself. This simplicity allows insight into the cause-and-effect relations of the physics being modeled; such insight was valuable during the development of aero-optical scaling laws discussed in Section 3.4 below. The justification for using the (inherently incompressible) DVM, its implementation details, and the resulting time-varying velocity fields are presented in APPENDIX D.

Given this correlated time series of instantaneous realizations of the velocity

field from the DVM, the problem of modeling the weakly-compressible aberration mechanism was taken up. Guided by suggestions in the literature, density changes in a weakly-compressible shear flow were initially modeled accounting for only the effect of adiabatic heating and cooling, consistent with Morkovin's Strong Reynold's Analogy (SRA).[46,47] The SRA suggests that static pressure fluctuations can be neglected, and thus index (i.e., density) became a function of velocity and total temperature *only*. This mechanism in a total-temperature-matched shear layer (like that at AEDC), however, produced a relatively benign index field and yielded a time series of OPDs that were totally incompatible with those measured at AEDC.[31,40]

Forced to explore other possible mechanisms, a model was developed which accounted for the pressure gradients which accompany streamline curvature (i.e., abandoning the SRA altogether). The pressure and concomitant density fields were found by (iteratively) integrating the unsteady Euler equations as detailed in Ref. 40. Our weakly-compressible model suggested that total temperature separations akin to those produced in Ranque-Hilsch tubes might also be present. The final weakly-compressible model was improved by incorporating the Ranque-Hilsch effect. Unlike the case of a compressible boundary layer,[46] results of this final weakly-compressible model showed that significant pressure fluctuations are present in a weakly-compressible shear layers, as illustrated in Fig. 8. While pressure fluctuations are the dominant factor producing optical distortions, the temperature-separation effect acts to reduce the amplitude of these distortions. Fig. 8 also shows the schlierens and wavefronts produced by the computed density fields.

This final weakly-compressible model produced excellent comparisons with the large-scale, dominant-amplitude aberrations observed in the AEDC experimental data. Further, the weakly-compressible model's index-of-refraction fields produced simulated schlierens which matched the character of experimental schlierens ubiqui-

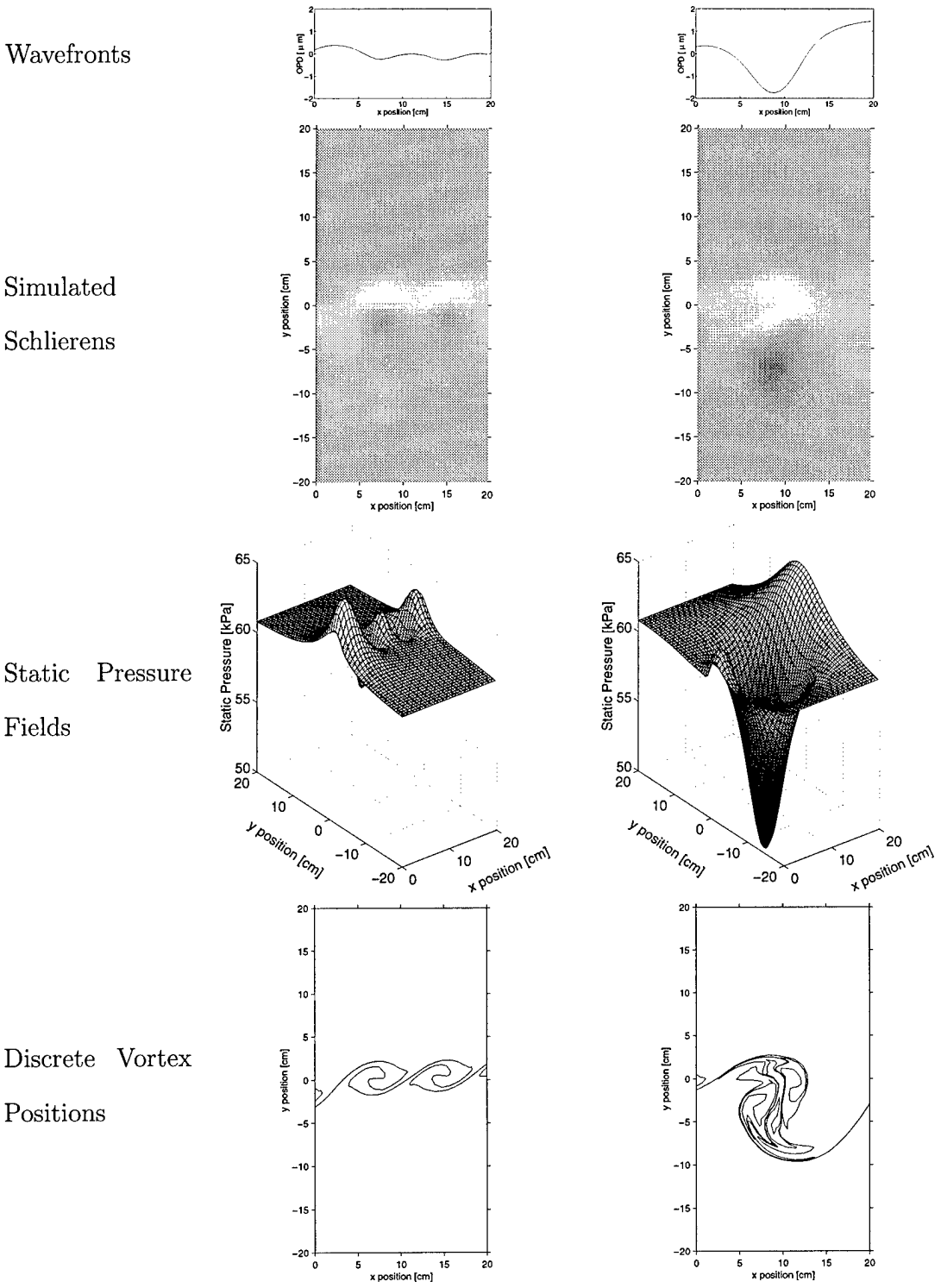

Figure 8. Compressible shear layer simulation at two time steps, one prior to pairing (left) and following multiple pairings (right).

tously reported in the literature (see Fig. 8). Once shear-layer roll-up occurred, in fact, these large-scale distortions were relatively insensitive to initial splitter-plate boundary-layer thickness.[31]

As described in Ref. 40, our simulation reasonably models the large-scale distortions measured by Hugo *et al.* in the compressible shear layer[18] as shown in Fig. 9. The small-scale structures measured in the AEDC *OPD*s are compatible with the notion that they are due to temperature discontinuities introduced into the shear layer at the splitter-plate and/or due to tunnel-access-window boundary layers. In either case, small-scale distortions would be superimposed on the large-scale distortions predicted by the weakly-compressible model. Evidence of this is shown in the station 1 wavefronts measured immediately downstream of the splitter plate (Fig. 9). Superpositioning the station 1 experimental data on our station 2 simulation produces wavefronts of similar character to those measured at station 2 as shown in Fig. 9.

The discrete vortex velocity model together with the weakly-compressible index-of-refraction model described above produced a reasonable estimate of the aero-optical distortions measured in the AEDC weakly-compressible shear layer.

3.4. Resulting Scaling Laws

The DVM/weakly-compressible-model methods, described above and anchored to the AEDC experimental data, provided a means of testing the validity of candidate scaling relations. These DVM/weakly-compressible-model results were taken as the "true" results. The scaling results, summarized below, are detailed in Chapter 6 of Ref. 31.

Aero-optical distortions were found to scale with a simple density ratio for cases when the Mach numbers of the two constituent flows were unchanged. As a consequence of this, distortion amplitudes decreased with increasing altitude, as

Station 2 Numerical Simulation

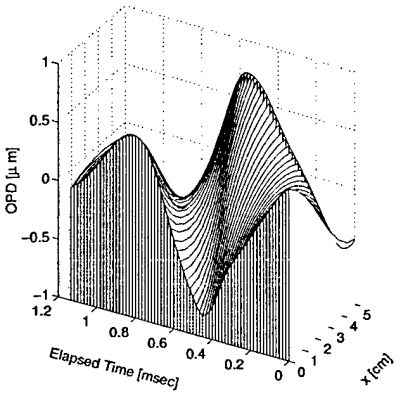

Station 1 Experimental Data

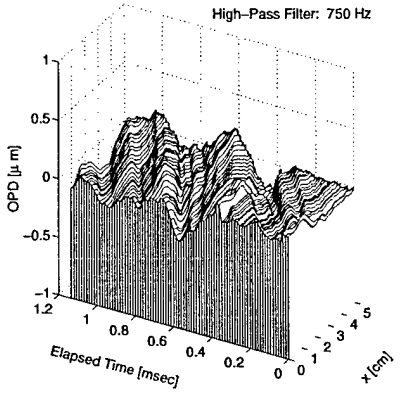

Simulation + Station 1 Experimental Data

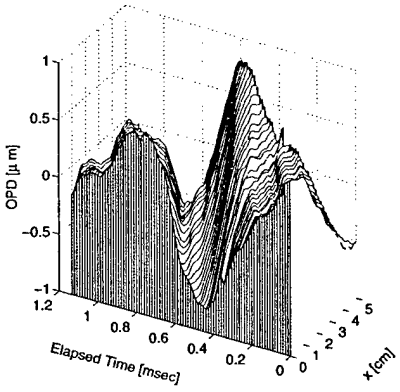

Station 2 Experimental Data

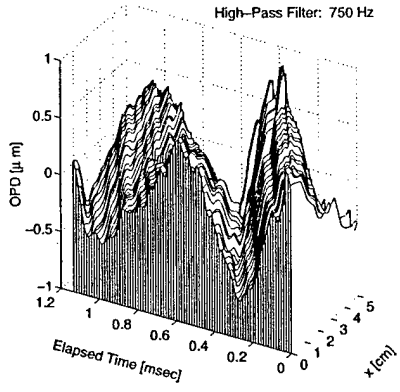

Figure 9. Comparison of wavefronts from discrete vortex simulation with superpositioned station 1 (experimental) wavefront to reconstructed experimental wavefronts for AEDC facility station 2.

shown in Fig. 10, causing an increase in time-averaged Strehl Ratio, $\overline{SR}$. The scaled results matched the "true" results to within a fraction of a percent for both mean and instantaneous OPD. Altitude variation changed the instantaneous amplitude of the distortion but not its spatial scales/shapes. The temporal frequencies of the distortion were reduced with the reduction in the constituent flow velocities required to maintain constant Mach with increasing altitude (through a rescaled time step). This suggests that the correction rate required by an adaptive-optic system would decrease by $\sim 10\%$ as altitude increased from 13,500 ft to 40,000 ft.[31]

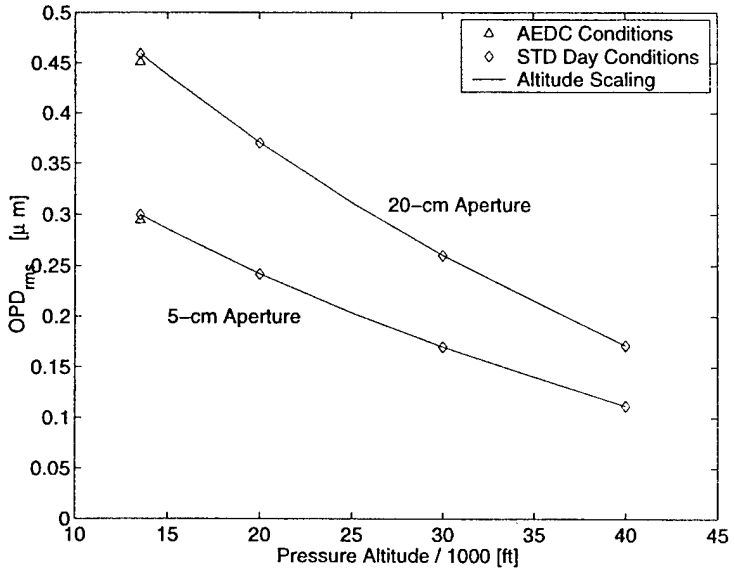

Figure 10. Effect of altitude on OPD_{rms} (Mach numbers fixed) as computed by weakly-compressible model (symbols) and using density ratio scaling law (lines) (AEDC station 2, $\delta_i/2 = 8.626$ mm)

An additional temperature ratio factor was required to scale aero-optical data collected at one altitude to another altitude for cases where the velocity difference of the constituent flows was held constant. Data scaled with this relation were within 4% of the results obtained for the "true" results both for instantaneous and mean OPDs. Distortion variation with altitude followed the same trends as for the constant-Mach

cases as shown in Fig. 11; however, distortion amplitudes were larger for the constant-velocity-difference cases due to the increase in Mach numbers which accompanies the reduction in the sonic speed with increasing altitude. In this case, wavefront temporal frequencies were unaffected by changes in altitude.[31]

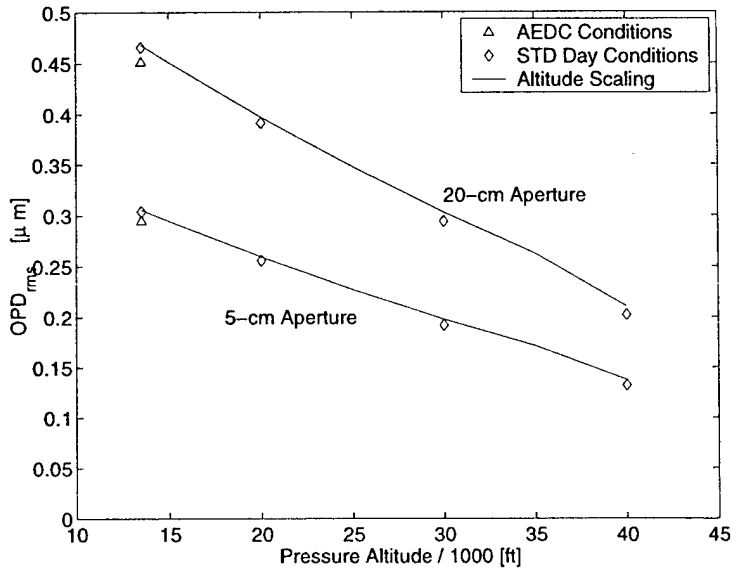

Figure 11. Effect of altitude on OPD_{rms} (velocity difference fixed) as computed by weakly-compressible model (symbols) and using combined density/temperature ratio scaling law (lines) (AEDC station 2, $\delta_i/2 = 8.626$ mm)

The OPD_{rms} data for the weakly-compressible model at different altitude conditions were compared to free-shear-layer (fence) and turbulent-boundary-layer data obtained in actual flight tests by Gilbert.[48] Incredibly, the weakly-compressible-model data agree with Gilbert's data to within the experimental measurement uncertainty as shown in Fig. 12. In addition, a quadratic fit of the weakly-compressible-model data provided a superior match over the linear relation suggested by Gilbert, although the general trends of both fits are similar.[31]

The scaling objective of this grant was prompted by the inability to scale the OPD structure sizes/frequencies of the heated jet measurements to those measured

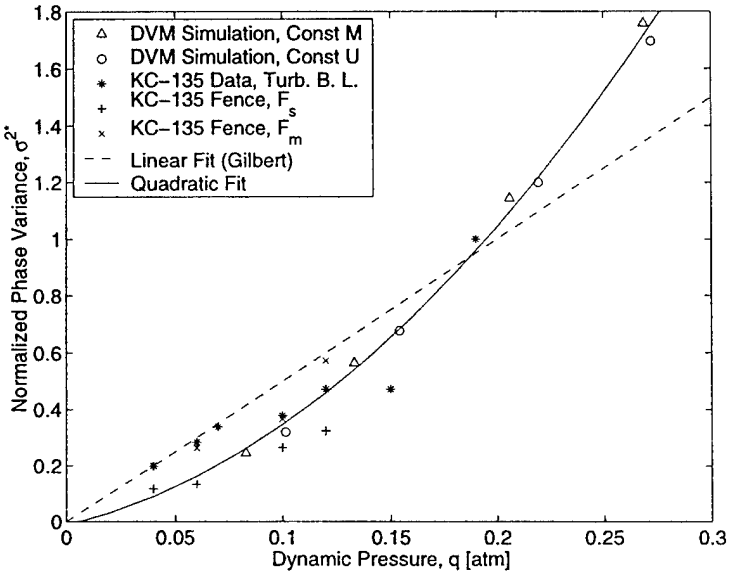

Figure 12. Effect of dynamic pressure, q_∞, on OPD_{rms}. KC-135 data taken from Ref. 48; DVM/weakly-compressible-model data from AEDC station 2, $\delta_i/2 = 8.626$ mm simulation.

at AEDC. The present grant's research showed that AEDC flowfield structure size, dominant temporal frequency, and maximum distortion amplitudes scaled as would be expected from the fluid-mechanics literature. This scaling is based on the primary coherent structures in the shear layer and thus *only* holds for an aperture sized larger than the largest flow structures. Since the AEDC data was obtained with an aperture smaller than this structure size, the scaling was only apparent by comparing the AEDC-anchored DVM/weakly-compressible-model results with those of the heated jet as shown in Table 1. The specifics of this scaling are detailed in Section 6.5 of Ref. 31.

4. TWO-DIMENSIONAL WAVEFRONT SENSOR

In the first grant, we demonstrated a high-bandwidth ($\sim$ 100 kHz) sensor which took advantage of the fact that aberrating, turbulent flow structures "convect" across

Table 1. Comparison of flowfield characteristics for two example shear flows: heated jet (dissimilar-index mixing) and weakly-compressible shear layer (DVM/weakly-compressible model)

Facility	Heated Jet (Ref. 6)	AEDC Shear Layer	Ratio = AEDC/Jet
Distortion Cause	$\Delta T = 50°C$	$M_1 \sim 0.8$, $M_2 \sim 0.1$	
Tested Aperture (cm)	1.27	20	~ 16
Equivalent D (cm)	1.27	20	~ 16
Equivalent x (cm)	3.18	48.3	~ 15
Equivalent x/D	2.5	2.4	~ 1
ΔU (m/s)	7	226	~ 30
U_c (m/s)	3.5	148	~ 40
Structure Size, Λ (mm)	6	~ 100	~ 16
$f_{\overline{OPL}}$ (Hz)	~ 500	~ 1500	~ 3
OPD_{max} (μm)	0.1	~ 1.5	~ 15

the viewing aperture.[6,13,18] This reliance on structure convection, however, limits the SABT to measurement of the streamwise component of the optical wavefront. For the two-dimensional derivative of the SABT, we used the streamwise convection to unfold the wavefront in the streamwise direction. In addition, we imposed a scan velocity in the cross-stream direction to unfold the remaining orthogonal component, thereby producing the full, two-dimensional wavefront as shown schematically in Fig. 13.

The testing of a breadboard implementation of the cross-stream scanner component revealed a measurable beam displacement inherent in the scanning process *alone*.[14] This displacement can be removed as a tare, provided it is repeatable. Thus,

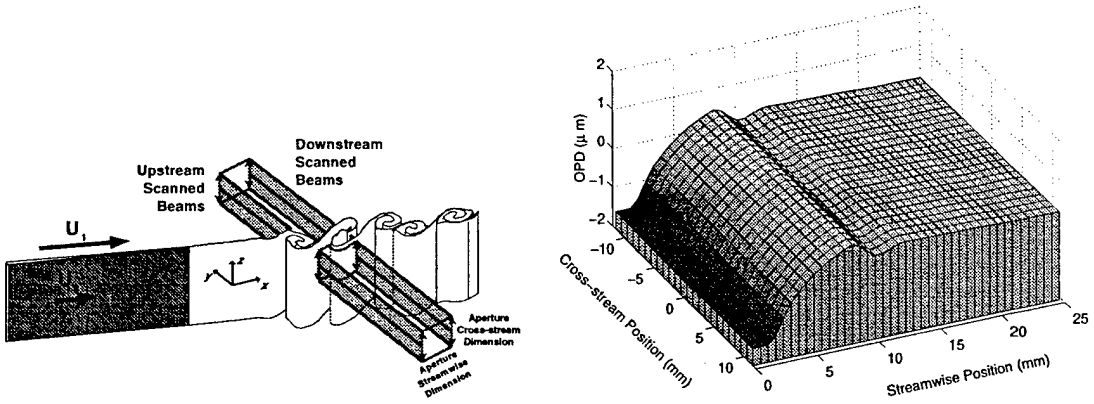

(a) (b)

Figure 13. Example (simulation) of (a) a two-dimensional flowfield and (b) the resulting two-dimensional optical wavefront over the aperture defined by the "upstream" and "downstream" beams. (From Ref. 15.)

a key to successful implementation of this instrument concept was the incorporation of a galvanometer scanner with position feedback control for high scan-to-scan repeatability.[15]

The SABT-derivative instrument was tested in the Notre Dame water tunnel. A mixing layer was produced by a vertically-mounted splitter plate at the upstream end of the test section as shown in Fig. 14 and detailed in Ref. 15. A velocity differential between the two sides of the plate was created by installing a "straw box" flow restrictor on one side of the plate and by modifying the tunnel inlet. A 1000-W cartridge heater, installed 11.4 cm ahead of the trailing edge, produced an optically-active flow. During this experiment, the flow on one side of the plate was $U_1 = 18.5$ cm/sec while the flow on the low-speed side was $U_2 = 4$ cm/sec. The flowfield is visualized with hydrogen bubbles in Fig. 15. Visible in Fig. 15 are vortical coherent structures in the mixing layer itself which are roughly equivalent to those

shown the two-dimensional flow example, Fig. 13. The resulting wavefronts were a time-resolved, time series; individual wavefronts were obtained at 600 Hz (two measurements per scanner cycle).[15] A series of these wavefronts (every 20th frame) is shown in Fig. 16. The bandwidth of this new wavefront sensor can be increased to 8 kHz by incorporating a faster scanner (already in hand). We plan to use the 8 kHz instrument for two-dimensional wavefront measurements in laboratory air flows.

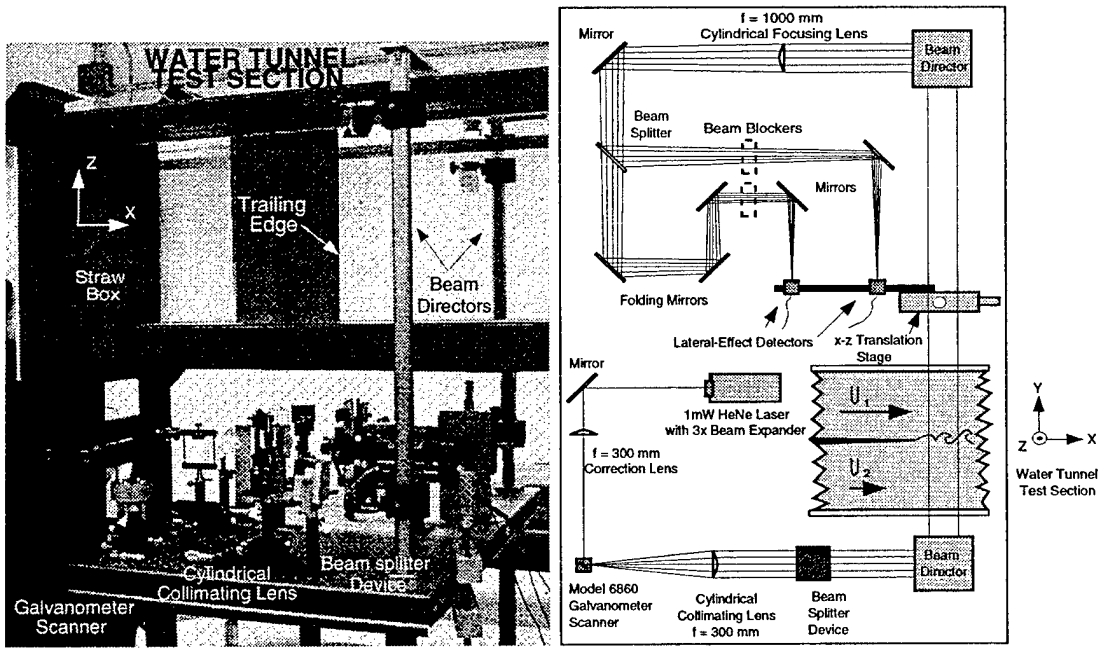

(a) (b)

Figure 14. (a) Photograph of water tunnel heated shear layer facility and (b) schematic of the SABT-derivative instrument optical bench.

5. SHEAR-LAYER CONTROL

The use of control for heated-jet experiments greatly enhanced certain areas of investigation in our previous work (see, for example, Refs. 49 and 50). The coupling of control with the SABT sensor suggests the possibility of not only real-time sensing of wavefront aberrations but also for adaptive-optic correction. An initial look at

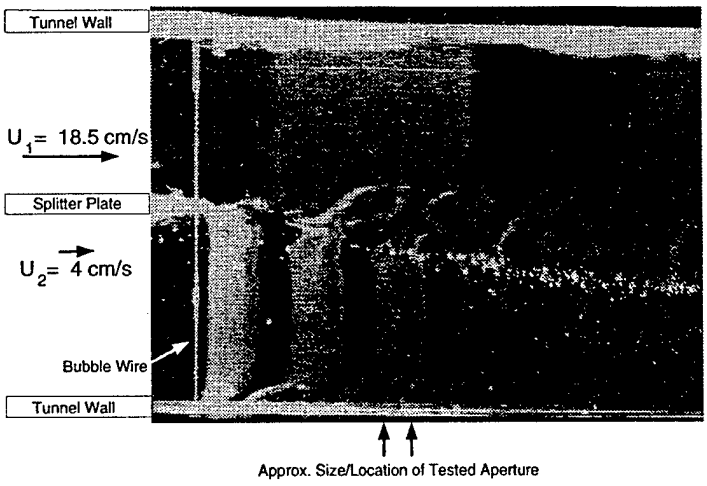

Figure 15. Hydrogen bubble visualization of heated mixing layer (looking up through the bottom of tunnel test section).

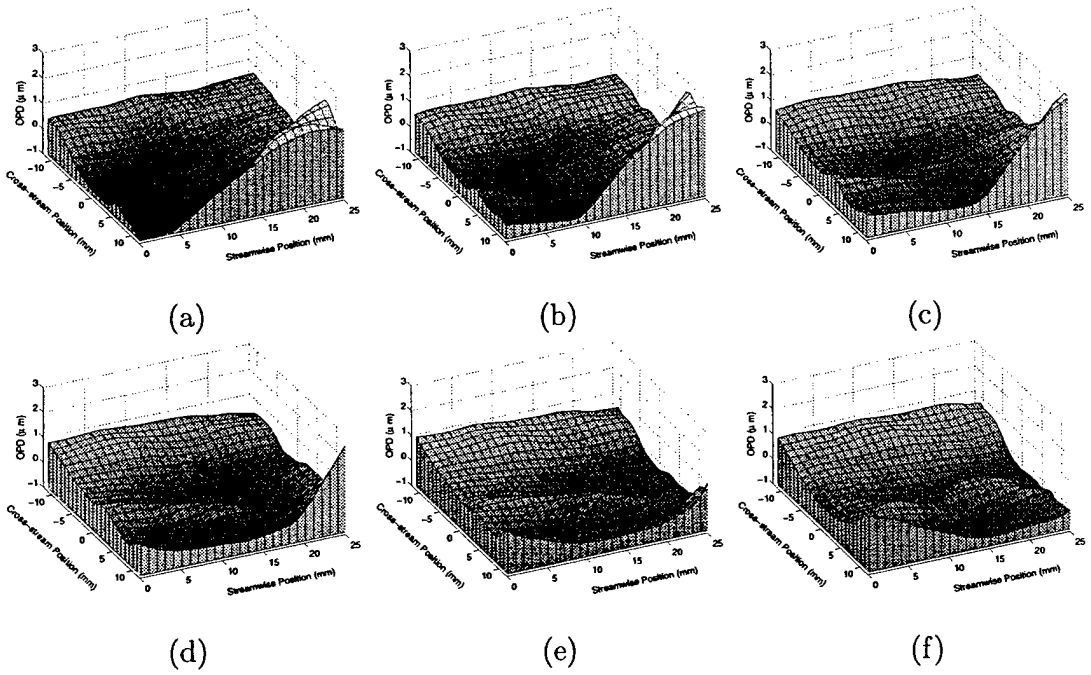

Figure 16. Experimental, two-dimensional, wavefront reconstructions: time steps = 924. (a) through 1024 (f). Between frames, $\Delta t = 0.0333$ sec; overall period (a)–(f) = 0.1667 sec.

the possibility of shear-layer control was performed during this grant using the DVM code.

For a free shear layer, the wavelength of the most unstable mode is driven by the layer's initial thickness according to linear stability theory[51,52] and the experimental literature.[53,54] In fact, we found that our DVM model followed the theory extremely well. The shear layer's natural frequency, f_n, can be predicted from the Strouhal number

$$St_0 = \frac{f_n \theta_0}{U_c} = 0.032 \tag{3}$$

where θ_0 is the momentum thickness of the high-speed stream at the splitter plate trailing edge (and assuming $U_c = (U_1 + U_2)/2$).[53,54] Shear layer rollup has been experimentally observed to occur at approximately $x = 3\lambda_n$ where the natural wavelength, λ_n, is given by[53,54]

$$\lambda_n = \frac{U_c}{f_n}. \tag{4}$$

Table 2 compares the shear layer natural frequencies and concomitant first rollups predicted using these relations for different initial discrete vortex core radii. (It should be noted that the length scale θ_0 used in Table 2 was the momentum thickness of the high-speed stream *only*, as stipulated in Ref. 53.) Table 2 shows that the DVM's initial rollup occurs at a position that varies with initial layer thickness and is consistent with theory and experiment. Moreover, if the shear layer is artificially perturbed at frequency f_n, the shear layer tends to rollup into "rollers" of length $\sim \lambda_n$ as shown in Fig. 17.

The streamwise energy content of the forced shear layer is typically quantified as[53,54]

$$E(f) = \int_{-\infty}^{\infty} \frac{[\mathbf{u}'(f)]^2}{2\theta_0} dy \tag{5}$$

where $u'(f)$ is the narrow-band velocity fluctuation level. When the energy content within each frequency band was computed from forced DVM velocity profiles, the

δ_i (mm)	θ_0 (mm)	f_n (Hz)	λ_n (cm)	Predicted Rollup (cm)	DVM Typical Rollup (cm)
69.00	5.250	901.29	16.41	49.22	$\sim$ 45–60
34.50	2.975	1590.80	9.30	27.89	$\sim$ 26–30
17.25	1.429	3310.79	4.46	13.40	$\sim$ 16–20

Table 2. DVM simulation of (unforced) AEDC-type shear layer: DVM rollup position compared to predictions using Ref.[54] methods (θ_0 for high-speed stream *only*)

energy at each frequency initially increased with increasing x, as shown in Fig. 18 for frequencies f_n and $f_n/2$. The energy content in the forcing frequency mode, f_n, increased until saturation occurred at the x corresponding to the shear-layer initial rollup. Beyond the initial rollup, the energy content at the subharmonic frequency $f_n/2$ dominated until it also saturated at the position corresponding to the first pairing of the vortex "rollers." This energy amplification behavior matches that noted in the experimental literature.

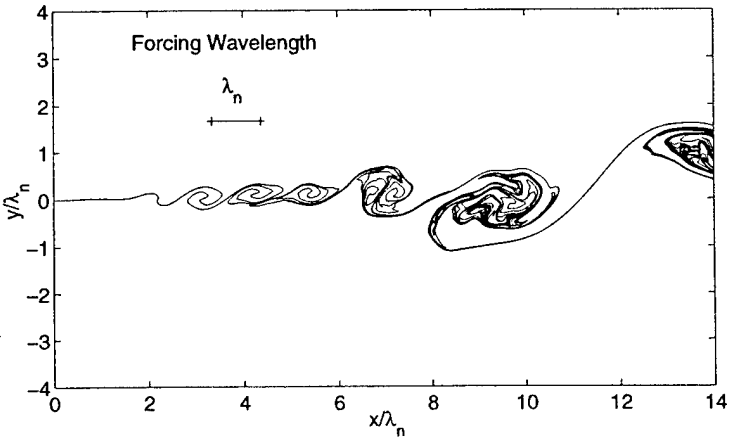

Figure 17. Locus of discrete vortex positions for *artificially forced* DVM shear layer, time step = 716 (AEDC conditions, $\delta_i = 34.5$ mm, forcing frequency, $f_n = 1591$ Hz)

The good agreement between the DVM simulation and the behavior of real

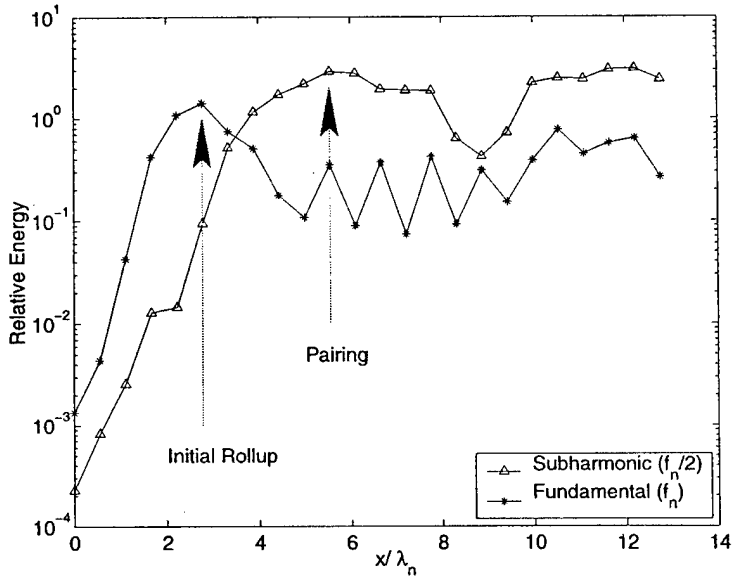

Figure 18. Streamwise energy content variation with x for *artificially forced* DVM shear layer (AEDC conditions, $\delta_i = 34.5$ mm, forcing frequency, $f_n = 1591$ Hz)

shear layers reported in the experimental literature suggest that the DVM is a useful tool for evaluating potential forcing schemes.

The problem of flow control at compressible velocities centers on having sufficient frequency response and actuator energy density. Electro-menchanical devices which can produce high enough amplitudes (electro-magnetic or bi-metallic pistons and flaps, for instance) typically lack sufficient bandwidth whereas those with high frequency response (piezoelectric, electrostatic) typically have low displacement amplitudes. Corke and Cavalieri[55,56] have used phased-plasma-array actuators for exciting instabilities in a Mach 3.5 boundary layer. These show promise for shear-layer control as well.

This problem of shear-layer control will be further explored both numerically and experimentally in our follow-on grant, AFOSR F49620-00-1-0025.

6. INFERRING FLUID-MECHANIC INFORMATION FROM WAVEFRONTS

Finally, some preliminary investigations into inferring fluid-mechanic information from the distorted wavefronts were undertaken in our first grant (see, for example, Refs. 21 and 57); however, in this objective, we have begun to investigate this relationship more formally by employing wavelet transforms and/or proper orthogonal decomposition methods to decompose the SABT signals. In so doing, we plan to develop algorithms for extracting the velocities for each of the aberration-causing flow structures. This work is the primary focus of our newest researcher and will continue in our follow-on grant, AFOSR F49620-00-1-0025.

7. DISSEMINATION OF RESULTS

7.1. Publications

This research has produced a Ph.D. dissertation (Ref. 31), six meeting papers (Refs. 21, 14, 15, 58, 40, and 30), and two journal articles (Refs. 16, 59). Refs. 60 and 32, versions of Refs. 15 and 30 (meeting papers), are currently in review by the journals *Optical Engineering* and *AIAA Journal*, respectively. Ref. 40 is currently being revised for submission to *Journal of Fluid Mechanics*. In addition, a tentative arrangement has been reached with the editor of *Progress in Aerospace Sciences* to publish an updated version of the "AIAA Plasmadynamics and Lasers Best Paper Award (1997)"-winning review paper (Ref. 21) funded under this grant.

7.2. Technology Transfers

In addition to presentations made at AFOSR-sponsored meetings and national technical meetings, we have endeavored to transition our findings to those who are

actively working in the aero-optics field. Recently, our research was presented by Dr. D. Kyrazis at the Second Annual Directed Energy Symposium (1–5 November 1999).[19] In addition, we have explored with Boeing the use of the SABT for ABL aero-optics ground tests and have offered to assist in developing an array of sensors for this purpose. We have also supported the hypersonic aero-optic testing performed in Calspan UB Research Center's Large-Energy National Shock facility.

8. PERSONNEL SUPPORTED UNDER THIS EFFORT

This grant provided approximately one month of support each year to the Principal Investigator, Dr. Eric J. Jumper. In addition, a full-time Ph.D. student, Edward J. Fitzgerald, was supported through his Ph.D. degree. A second Ph.D. student, James Cicchiello, was also supported during the last year of the grant.

APPENDIX A. AERO-OPTIC STATISTICAL APPROACH

An early, if not the first attempt to quantify the aero-optical aberration imposed by propagation of a collimated coherent beam of light through an optically-active (index-of-refraction variant) turbulent flowfield was that by Liepmann.[8] The motivation for this first study was to place some limits on the sensitivity (i.e., sharpness) of Schlieren systems for use in high-speed flow analysis. Liepmann analyzed the propagation of a small-aperture (small-diameter) beam and derived its mean-square deflection angle off its mean angle, $\langle \epsilon^2 \rangle$, using geometric optics. After propagating through a boundary layer of thickness d, in the propagation direction y, where changes in the index of refraction in the normal plane, x–z, are taken to be statistically similar, Liepmann's analysis gave

$$\langle \epsilon^2 \rangle = \frac{1}{[n_0(\delta)]^2} \int_0^\delta \int_0^\delta n_0(x)\, n_0(\xi)\, \langle \left(\frac{\partial \upsilon}{\partial y} \right)^2 \rangle\, R_\upsilon(\mid y - \zeta \mid)\, dy\, d\zeta \tag{6}$$

where the index of refraction is given by $n = n_0(y)(1+\upsilon)$, and $R_\upsilon(\mid y-\zeta \mid)$ is the correlation function for the index variation. When the index-of refraction fluctuation, υ, is replaced by the density fluctuation, ρ', using the Gladstone-Dale constant, K_{GD},[22]

$$\upsilon = \frac{\rho' K_{GD}}{n_0} \tag{7}$$

Eq. 6 becomes

$$\langle \epsilon^2 \rangle = \left[\frac{K_{GD}}{n_0(\delta)} \right]^2 \int_0^\delta \int_0^\delta \langle \left(\frac{\partial \rho'}{\partial y} \right)^2 \rangle\, R_{\rho'}(\mid y - \zeta \mid)\, dy\, d\zeta \tag{8}$$

It is of interest to note that this early work introduced concepts that remain important to aero-optics; first, Eqs. 6 and 8 introduce the notion of linking statistical measures of the turbulent flowfield to the time-averaged optical degradation. Further, they introduce the correlation function or "scale of the turbulence" and its position dependence along the propagation direction as key to evaluating the statistical aero-optical effect.

A significant piece of work was done in 1956 by Stine and Winovich;[61] they performed photometric measurements of the time-averaged radiation field at the focal plane of a receiving telescope that imaged an initially planar light wave apertured by pinholes ranging in diameter from 0.75×10^{-3} to 33.0×10^{-3} inches. This experimental data was used to assess Liepmann's analysis as well as that performed at Northrop Aircraft by Baskins and Hamilton on the transmission characteristics of an optical signal through supersonic, turbulent boundary layers.[62,63] Stine and Winovich's work is important on several accounts. It brought together all that had been done till then on optical propagation through index-variant turbulent flow. In addition, it brought to bear on the problem the relatively mature analysis of electro-magnetic scattering in the troposphere and through atmospheric turbulence[64,65] which would continue to be of importance to aero-optics. This work also raised the prospect of using an optical degradation measurement as a method of inferring turbulence scales; this hope of being able to infer information about the turbulent flowfield from optical measurements of aero-optic effects remains as one of the potential fluid-dynamic payoffs that may come from aero-optic research.

In my opinion the milestone paper in "modern" aero-optics is that by Sutton;[2] this paper set several trends that dominated the study of statistical aero-optics in the "modern" era. By "modern" I mean here the effect of aero-optics on the beam quality of high-power laser irradiation. The aero-optic problems in the laser applications are ubiquitous, and the combined fluid-mechanist and laser-physicist communities began to get serious about dealing with the problems. The Sutton paper was the first paper to consider the problem of the effect of near-field phase aberrations due to the propagation of a large-aperture, single wavelength, collimated (planar-wavefront) beam through a turbulent, optically-active, spatially-confined flowfield. Imbedded in the analysis was the first time the linking equation relating optical phase variance

over the exit pupil to specific fluid-mechanic properties was advanced in the form of a position dependent (along the propagation path) extinction coefficient, α,

$$\alpha = 2k^2 \langle v^2 \rangle \Lambda \tag{9}$$

in the Lambert's law sense for a reduction in intensity, I, as

$$\frac{dI}{dy} = -\alpha I \tag{10}$$

where $k = 2\pi/\lambda$, λ being the wavelength of the radiation. When integrated over the thickness of the flowfield, L, Eq. 9 yielded the mean-square phase error, σ_ϕ^2 as

$$\sigma_\phi^2 = 2k^2 \int_0^L \sigma_{v'}^2 \, l_y \, dy \tag{11}$$

where Sutton suggested that the proper correlation length scale, l_y, should be Λ, the position-dependent integral scale size of the turbulence.[66] If the Gladstone-Dale constant is introduced as above, Eq. 11 becomes

$$\sigma_\phi^2 = 2K_{GD}^2 \, k^2 \int_0^L \sigma_{\rho'}^2 \, \Lambda(y) \, dy. \tag{12}$$

The paper also introduced the now common use of the mean-square phase error to directly estimate of the far-field intensity reduction or Strehl ratio[1]

$$SR = \frac{I(0,0)}{I_0(0,0)} \tag{13}$$

via the large-aperture approximation to obtain the time-averaged Strehl ratio as

$$\overline{SR} = \exp(-\sigma_\phi^2). \tag{14}$$

From the time of that paper on, the focus and content of aero-optic research was shaped. A review of the major publication in aero-optics, *Aero-Optical Phenomena*,[67] demonstrates that work up until 1982 focused on the measurement of the time-averaged, spatial, near-field optical phase variance, σ_ϕ^2. Measurements of σ_ϕ^2 were

obtained either by direct optically-based methods (Ref. 68, for example), or indirectly using fluid-mechanic measurements via the linking equation of Eq. 12 (Ref. 69, for example). Optical methods that have been applied to the measurement of the near-field time-averaged phase variance include direct interferometry, pulsed interferometry[68] and shearing interferometry.[70] These interferometric methods provide a time-averaged assessment of the optical phase variance over the aperture by quantifying the phase variance of individual interferograms and averaging the variance over the number of interferograms used to quantify the aperture aberrations. Individual interferograms are uncorrelated, so that, given a sufficient number of interferograms, the estimates of the time-averaged phase variance can be expected to yield accurate results; however, these methods provide no information concerning temporal frequencies.

Indirect methods of assessing the near-field optical phase variance via Eq. 12 depend on a quantification of the density fluctuations which are generally experimentally measured using hot-wire methods.[2,69] Since a complete quantification of a two-point correlation is time consuming, Rose *et al.*[69] developed further assumptions regarding the form of the covariance function of the density fluctuations to reduce the required sampling time of the measurements. Again these methods provide no temporal information about the near-field phase variance. Many efforts were directed at comparing the inferred phase variance from fluid-mechanic linking equations and the optically-measured (inferred) time-averaged phase variance. As recently as 1992, a paper was presented reviewing the analytic linking methods used to infer optical wavefront variance.[9]

To end this brief and incomplete historical review, I refer to a final paper, again by Sutton, published in 1985.[66] I do not presume to judge the intent of that paper; however, to this reader, the paper suggests that the field of aero-optics was essentially mature, and that the opportunities for further research were to polish up

the techniques already in existence and maybe apply them to a few more flows. I should note that, in fact, work continues to this day on dotting the i's and crossing the t's of the traditional methods of assessing near-field phase variance. In the end, however, the now-traditional methods in aero-optics are limited in their ability to take an active role in system design and performance. As the field of aero-optics has been described, the best that can be hoped for is an ever more accurate assessment of the optical degradation that may be expected (in a time-averaged sense) for a given set of flow conditions. These methods do not suggest either the temporal or spatial frequencies associated with the optical aberrations and, more importantly, they do not even provide a close approximation of the instantaneous near-field optical wavefront distortions. In terms of providing design specifications for adaptive-optical systems, the traditional aero-optics approaches are of little to no value; in other words, as represented up to 1992, aero-optics was at a level-one understanding and content to be there.

APPENDIX B. FIRST DIRECT OPTICAL MEASUREMENT OF OPD_{RMS}

The first instrument to address dynamics of aero-optics was developed by Malley *et al.* in the late 1980's,[10] although their intention was only to obtain a statistical measure of OPD_{rms}. Their concept first appeared in print in 1989.[11] In these papers, Malley, *et al.* describe the invention of a relatively inexpensive and quick optical method for assessing the statistical, optical phase variance. Key to their method was Malley *et al.*'s assertion that optical aberrations imposed by a convecting, optically-active turbulent flow must themselves "convect" through the viewing aperture. In their writings this assertion is stated almost cavalierly, as if it were common knowledge, and so, upon thinking about it, it would seem; however, this assertion must be cited as one of the pinnacle discoveries of the new dynamic era in aero-optics. With this recognition, a spatially-stationary time series of wavefront, spatial-derivative measurements can be used to determine an accurate statistical measure of the wavefront distortion over a relatively-large region of the viewing aperture near the point where the derivative measurement is made. I will return specifically to Malley *et al.*'s method; however, first I want to explore the ramifications of their discovery.

B.1. Hartmann Sensor Theory

A common method of measuring the figure of an optical wavefront is by employing a Hartmann wavefront sensor.[12] According to Huygen's principle[71] a ray of light travels normal to its associated optical wavefront; this principle is, in fact, the basis for geometric optics. As shown in Fig. 19 (greatly exaggerated), if a planar wavefront is made to propagate through an aberrating medium (due to density fluctuations, for example), the wavefront emerges distorted or aberrated. Note in Fig. 19 that there are a number of vectors shown normal to the emerging, aberrated wavefront,

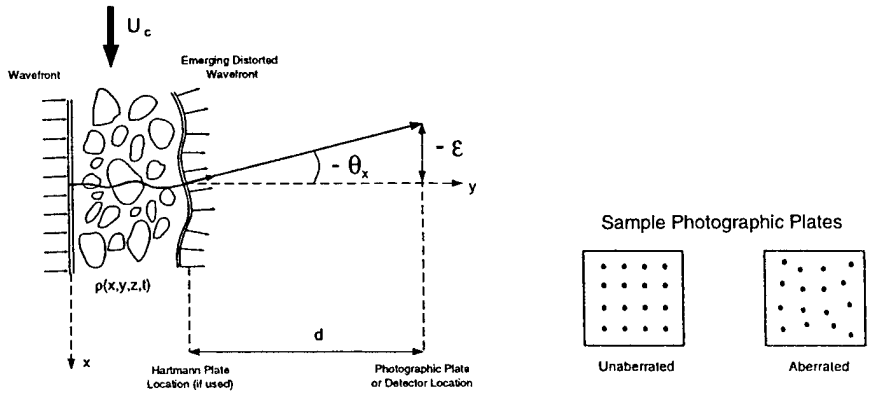

Figure 19. Planar wavefront and probe beam distorted by a variant fluid density field (left) and resulting Hartmann Sensor dot displacements (right).

and also the path of a single "ray" as it traverses the medium and emerges normal the wavefront. In a classical Hartmann Plate, an opaque plate with an array of small-diameter (small-aperture) holes in it is placed at the point where the wavefront emerges from the aberrating medium, forming as many small-aperture beams as there are holes in the plate. Each hole in the Hartmann Plate defines the centroid of a subaperture of the full viewing aperture. Because of Huygen's principle, these beams will emerge from the plate at an angle normal to the plate-impinging wavefront at the location of the hole. As shown in Fig. 19, If a photographic plate is placed at some distance d from the plate in the y direction, and exposed for a very short time, the photographic plate will record the displacement of each beam from its null position. The null position can also be recorded onto the photographic plate by exposing the plate to the small-aperture beams emerging from the Hartmann Plate with no aberrating medium present. An example of the unaberrated and aberrated photographic plate might look like those in Fig. 19. If the distance in the y-direction of the photographic plate from the Hartmann plate is d, and the displacement of the dot from one small-aperture beam from its null position in the x direction is ϵ_x, then θ_x, the off-planar angle of the wavefront in the x–y plane, at the location where the

wavefront impacts the Hartmann plate can be determined, referring to Fig. 19, by

$$\theta_x = \arctan\left(\frac{\epsilon_x}{d}\right). \tag{15}$$

If θ_x is small, as it will normally be, then

$$\theta_x = \frac{\epsilon_x}{d}. \tag{16}$$

θ_x is the derivative of the wavefront in the x-direction in the x–y plane normal to the incoming wavefront direction at the Hartmann Plate. As described in Ref. 12, the relative wavefront (relative Optical Path Length, OPL) in the x direction can be constructed approximately by

$$OPL(x_j) \approx \frac{1}{d}\sum_{n=2}^{j+1}\left(\frac{\epsilon_{x_{n-1}} + \epsilon_{x_n}}{2}\right)(x_n - x_{n-1}), \tag{17}$$

where x_1 is the location of the first hole in the Hartmann Plate at $x = 0.0$, x_2 in the next location, etc., and x_j is the location of the jth of N holes in the x-direction in the Hartmann Plate. The reason that this equation is approximate is that it represents a discretized approximation to the integral

$$OPL(x_j) = \int_0^{x_j}\left(\frac{dOPL}{dx}\right)dx. \tag{18}$$

The validity of the approximation depends on the distance between holes, $(x_n - x_{n-1})$, being small compared to the change in the slopes of the wavefront. A similar approach using the displacement of the dots on the photographic plate from their null positions in the z-direction, ϵ_z, gives $OPL(z)$. Complete constructions of $OPL(x)$ and $OPL(z)$ over the viewing aperture yields a two-dimensional wavefront at the instant in time at which the photographic plate is exposed, $OPL(t, x, z)$.

If, instead of a photographic plate, the plate is replaced with a charge-coupled device (CCD) array, and the Hartmann Plate is replaced by an array of lenslets (each lenslet defining a subaperture), the wavefront sensor is termed a Shack-Hartmann

sensor. This sensor is capable of making wavefront measurements at the framing rate of the CCD array. The standard video framing rate is 30 Hz, but research-class, state-of-the-art CCD arrays can frame, i.e., interrogate every *pixel* in the CCD array, in approximately 1/1000 sec, or a rate of 1 kHz, to produce a time series of $OPL(x, z, t)$. Such wavefront sensors are now in common use in adaptive optic systems for the atmospheric propagation problem.

Malley *et al.*'s discovery recognized that if the aberrations were convecting (unchanging), then the required closely-spaced individual measurements of the wavefront derivative, in the form of off-axis, small-aperture-beam displacements could be replaced by a time series of off-axis displacements at a single location. This time series could then yield an optical pathlength as a function of time because

$$OPL(t) = \int_{t_0}^{t} \left(\frac{dOPL(t)}{dx} \right) U_c \, dt, \tag{19}$$

where $\frac{dOPL(t)}{dx}$ is just $-\theta_x(t)$, the continuous time series of off-axis displacement angles (given by Eq. 16) in the convection direction, and U_c is the $\frac{dx}{dt}$ of the "convecting" wavefront aberration. The discretized version of Eq. 19 is

$$OPL(t_N) \approx \sum_{i=1}^{N} -\Big[\theta_x(t_i) U_c \, \Delta t\Big]. \tag{20}$$

Given the relation of Eq. 19, Hugo[22] reexamined Liepmann's linking equation of Eq. 8 (of Appendix A). Using a Taylor hypothesis so that the derivative in Eq. 8, for example, can be replaced by

$$\frac{\partial \rho'}{\partial z} = -\frac{1}{U_c} \frac{\partial \rho'}{\partial t} \tag{21}$$

and incorporating Malley *et al.*'s discovery relating local tilt and U_c and integrating with time to arrive at $OPL(t)$, an equation can be developed following Liepmann's derivation of the form

$$\sigma_\phi^2 = K_{GD}^2 \, k^2 \int_0^\delta \int_0^\delta \mathrm{Cov}_{\rho'}(y - \zeta) \, dy \, d\zeta. \tag{22}$$

When the definition of the covariance function is inserted into Eq. 22 and integrated, it becomes

$$\sigma_\phi^2 = 2K_{GD}^2\, k^2 \int_0^L \sigma_{\rho'}^2\, \Lambda(y)\, dy \tag{23}$$

which is seen to be identical to Eq. 12 of Appendix A. Thus, Malley *et al.*'s discovery had implications that "unified" the traditional approaches to aero-optics as well as marking a turning point in the study of aero-optic phenomena.

B.2. The Malley *et al.* Device.

In Ref. 10 a device developed by Malley *et al.* was described that was able to make direct optical measurements of optical phase variance in near real time. As mentioned above, the device was based on their assertion/discovery that the optical aberrations caused by an optically-active turbulent fluid medium convect with the convecting flow structures. The device was cleverly simple and made use of an off-the-self electronic autocollimator. By monitoring the voltage fluctuations from the collimator they were able to record a time series of the off-axis displacement (jitter) of the centroid of a small aperture laser beam. The beam originated at the autocollimator and returned from a reflection off a flat mirror on the opposite side of the aero-optic disturbance. As discussed above, this beam jitter was directly related to beam off-axis angle variations (θ_x and/or θ_z). This small angle is the spatial derivative of the wavefront at the location of the small-aperture probe beam at the time associated with that measurement in the time series. As pointed out by Malley *et al.*, once the time series is available, Fourier techniques provide a direct measure of the OPD variance as a function of frequency.

Invoking a Taylor frozen-flow hypothesis allows for the spatial frequency, k, to be obtained from the temporal frequency via $k = \omega/U_c$, where ω is the temporal frequency. Thus, the instrument provided a measure of OPD variance both as an

integrated total and as a function of spatial frequency.

Although statistical (or perhaps better stated as, on a statistical basis), the data obtainable from the Malley *et al.* device, contained far more aero-optical information than had ever been previously available. It also compared well (was validated by comparisons) with the direct optical measurement of the OPD_{rms} inferred from averaging many instantaneous realizations of the flowfield via interferometry. In one step, aero-optics had advanced to a level-two understanding and completely bypassed the requirement for a linking equation like Eq. 12. Later work by Hugo[22] confirmed the high accuracy of the Malley *et al.* device in measuring OPD_{rms}.

APPENDIX C. THE SABT SENSOR DEVELOPED UNDER THE FIRST FUNDING ROUND

A new, very high-bandwidth wavefront sensor was developed under our first round of AFOSR funding. Refs. 6 and 13, describe a technique of making use of Malley *et al.*'s convecting aberration discovery, and multiple probe beams to develop a sparse-detector, high-speed wavefront sensor. To demonstrate the technique, a computational simulation of a two-dimensional heated jet was used. We explored the feasibility of using multiple, small-aperture, probe beams placed along the streamwise direction to use a variation of Eq. 20 from Appendix B, in constructing a wavefront of a would-be large-aperture collimated beam traversing the same flowfield at an instant in time. Our method made use of time-series data of the wavefront derivatives at the probe-beam locations "measured" both prior to and after the desired "construction" time. Although it appears to be a straight-forward exercise, embedded in the derivation of Eq. 20 is the fact that the fluid structures that give rise to the "convecting" optical aberrations on the wavefront are not frozen (i.e., the structures evolve).[6,13] In addition, the convection velocities change with time and from structure to structure (more than one of which's aberrating footprint is always present in the wavefront). Fig. 1 (in the main text of this report) is a time series of one-dimensional wavefronts (X/D is the nondimensionalized distance in the flow direction) due to propagation through the numerical heated-jet flowfield of Ref. 13. The X/D-vs-time slopes of the hills and valleys indicate the convection velocities of the aberrations on the wavefront, and the amplitude of the OPD vs. X/D gives the structure of the aberrations on the wavefront. Examination of these features in Fig. 1, demonstrate the facts that the convection velocities are time-varying and the aberration structures evolve in time; thus the frozen-flow hypothesis inherent in Eq. 20 is not strictly true. As described in Ref. 13, cross-correlation techniques between adjacent probe

beams can be used to obtain both a running estimate of the convection velocities and the evolution rates; these allow for the construction of a time series of time-resolved wavefronts, and the ability to place estimates on the accuracy of the measurements, respectively. Wavefront sensors developed using these methods are now referred to as SABT (Small-Aperture Beam Technique) wavefront sensors. SABT sensors have demonstrated a bandwidth of 100 kHz[17,18] and have been applied to optical wavefront measurements for propagation through heated jets,[6] compressible shear layers,[18] and heated-water shear layers.[15] To date the SABT wavefront sensor is the fastest wavefront sensor yet available; its high bandwidth is directly attributable to the fact that it is a sparse-detector sensor. The sparseness of the sensor means that the required number of interrogations to acquire the information to construct a full-aperture wavefront is reduced by one to two orders of magnitude from that required to obtain the same resolution from a Shack-Hartmann wavefront sensor.

APPENDIX D. SHEAR LAYER VELOCITY FIELD SIMULATION

The initial, transitionally-turbulent flowfield in a shear layer is dominated by the shear-layer rollup caused by the inviscid Kelvin-Helmholtz instability mechanism.[41] This rollup has been successfully simulated using various inviscid and pseudo-inviscid methods.[42–45] The shear layer for the present study was modeled using the discrete vortex method (DVM). DVM's are traditionally applied to incompressible flows because they rely on the global influence a discrete vortex induces on the flowfield through the Biot-Savart law. In a compressible flow, the speed of sound, a, is finite so this influence would be expected to travel along characteristic lines.[46] Trying to incorporate compressible effects into the DVM, though perhaps possible in principle, would add considerable complexity and significantly increase the computational demands of the simulation. On the other hand, within certain Mach-number restrictions, experimental observations of compressible shear layers (such as those in Refs. 34, 37, and 39) have found similar vortex structures and mean velocity profiles to those found in incompressible shear layers. Thus, there must be some validity to applying DVM directly to a weakly-compressible shear-layer flow. This validity is worth exploring further.

D.1. Evidence of Weak Compressibility

The Biot-Savart Law is a consequence of decomposing the velocity $\mathbf{V}$ of fluid particles in an infinitesimal control volume into rotational and irrotational parts.[72] It can be shown (see Refs. 31 and 40, for example), that the effect of compressibility, is to introduce a dilatation source term Δ into the irrotational part of the decomposition. This term is ultimately neglected in DVMs as they are normally implemented. Since the mean velocity profiles become self-similar for x corresponding to AEDC stations 2

and 3, any mean portion of Δ would vary only slowly in the $x-$direction; therefore, we would expect only an optical "piston" aberration or perhaps a slight tilt aberration which could be neglected. The order of magnitude of the fluctuating portion of Δ can be found from the fluctuating divergence, $\nabla \cdot \mathbf{u}'$, where $\mathbf{u}'$ is the fluctuating portion of $\mathbf{V}$ resulting from a Reynolds-type decomposition.[46] According to Smits and Dussauge,[46] the ratio of the fluctuating divergence to the magnitude of the velocity gradients of the energy-containing eddies, u'/Λ, is given by

$$\frac{\nabla \cdot \mathbf{u}'}{u'/\Lambda} \approx 10(\gamma - 1)M_t^2 \tag{24}$$

where γ is the ratio of specific heats for the gas, $M_t = \sqrt{\overline{u'^2}}/\bar{a}$ is the turbulent Mach number, and overbars signify time averages. For the AEDC flowfield, $M_t \approx 0.09$ whereby

$$\frac{\nabla \cdot \mathbf{u}'}{u'/\Lambda} \approx 0.03 \ll 1 \tag{25}$$

suggesting that the compressibility is weak and the fluctuating divergence might be neglected.[46,73]

Experimental condsiderations also argue that Δ has only a second-order effect on the AEDC velocity field. Mixing layers can be characterized by the convective Mach number M_{c1} of the largest flow structures. M_{c1} is defined as[39]

$$M_{c1} = \frac{U_1 - U_c}{a_1} \tag{26}$$

where U is the velocity in the x-direction, a is the speed of sound, and the convection velocity U_c is given by

$$U_c = \frac{a_2 U_1 + a_1 U_2}{a_1 + a_2}, \tag{27}$$

where 1 and 2 refer to the high- and low-speed streams, respectively. For the conditions tested by Hugo *et al.* at AEDC, the high-speed side of the shear layer was only $M_1 = 0.8$;[18] this means there were no shocks in the flow. Additionally, with a

low-speed side of 0.1 Mach, the convective Mach number M_{c1} seen by the largest-scale flow structures would be only $M_{c1} \approx 0.33$ for this case.[33,38] Further, it has been shown[38,37] that for compressible mixing layers with subsonic M_1, the reduction in visual spreading rate δ_{viz}/x (measured from schlieren photographs) for the compressible mixing layer relative to the incompressible case $(\delta_{viz}/x)_{inc}$ is less than 10% as shown in Fig. 20.

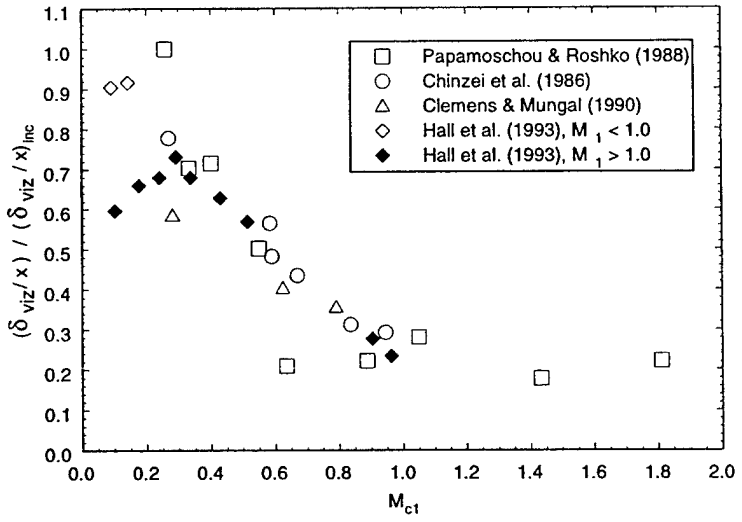

Figure 20. Normalized δ_{viz} growth rate variation with M_{c1}. Original data compiled in Fig. 9 of Ref. 37.

The shear layer's spreading rate can also be defined in terms of the growth with increasing x of the vorticity thickness δ_ω given by[34]

$$\delta_\omega = \frac{U_1 - U_2}{(\partial U/\partial y)_{max}}. \tag{28}$$

The (compressible) vorticity thickness spreading rate, δ_ω/x, for this M_{c1} actually remains unchanged from the incompressible spreading rate as shown in Fig. 21. More-elaborate, compressible numerical simulations also have shown that changes in shear layer structure do not occur at low M_{c1}.[24,25,74] Thus, it appears that the effect of compressibility might be reasonably neglected in the approximation of the (irrotational

part of the) velocity field for the AEDC test conditions.

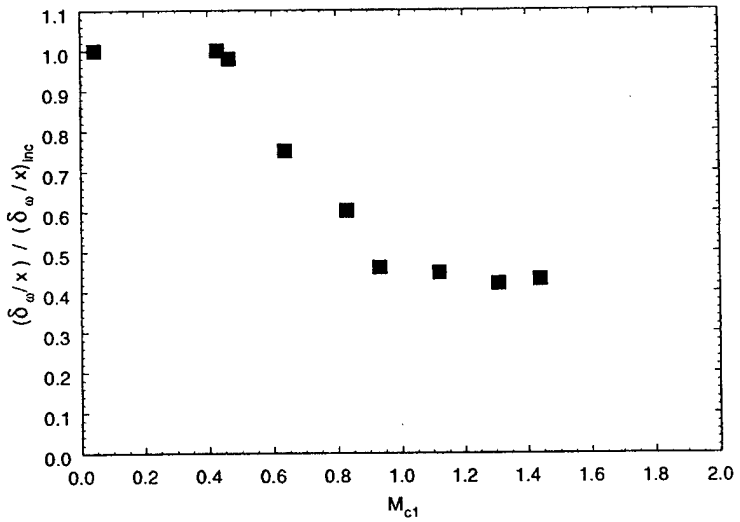

Figure 21. Normalized δ_ω growth rate variation with M_{c1}. Data as compiled in Fig. 17 of Ref. 39.

D.2. Velocity Field Model

The shear layer for the present study was modeled using the discrete vortex method, a technique first performed by Rosenhead.[75] The method has been subsequently refined using finite-core point (line) vortices[76] and redistributing the vorticity by inserting additional vortices as the vorticity-induced velocity fields spread the vortex elements apart.[13,77,78] Although an inviscid calculation, momentum diffusion was modeled by a temporal growth in the size of the rotational cores of the discrete vortices.[22,43] The primary advantage of using a discrete vortex method is its ability to model a shear flow with a fairly small computational domain thereby producing considerable computational savings. Modeling the shear layer using multiple vortex layers gives the capability of representing any arbitrary velocity profile across the shear layer.[78] Hugo used only a single vortex layer for each side of his jet to minimize the computational demands of the model.[13] Despite the relative crudeness of this model, Hugo's shear

layer structure agreed reasonably well with those of Ghoniem's[45] multiple layer model. Hugo's numerical simulation produced reasonable qualitative and quantitative agreement with his experimental heated jet. A more complete discussion of discrete vortex methods is given in Chapter 4 of Ref. 22.

The velocity fields for all cases of the present study were produced by a single, infinite shear layer modeled with discrete vortices in a manner similar to Hugo.[13,22] The splitter plate and shear layer near the plate trailing edge were modeled by discrete vortices. The influences of vortices far from the plate's trailing edge were modeled analytically. The splitter plate vortices' positions were indexed by one temporally-consistent position which, in effect, kept the splitter plate configuration fixed; once an individual plate vortex was indexed past the trailing edge, it became another shear layer vortex and was allowed to convect with time due to the net induced velocity at its position produced by all the other vortices in the model. The velocities on each side of the splitter plate, $U_1 = 261.04$ m/s and $U_2 = 34.7$ m/s, were chosen to match those of the AEDC shear layer. These yielded an initial circulation density, γ_d, for the vortices of $\gamma_d = U_2 - U_1 = -\Delta U = -226.34$ m/s and an imposed convection speed $U_{cn} = (U_1 + U_2)/2 = 147.9$ m/s. The velocity ratio across the shear layer was $r = U_2/U_1 = 0.132$. The initial vortex core diameter δ_i for the free vortices was varied to model different splitter-plate-boundary-layer thicknesses; during this study, $\delta_i = 17.25$, 34.5, and 69 mm. With an initial core diameter and a core growth rate function based on the growth rate of a laminar shear layer, the (instantaneous) shear layers shown in Fig. 22 were produced.

The mean velocity profiles can be collapsed by suitably nondimensionalizing the velocity[79]

$$U^* = \frac{U - U_2}{U_1 - U_2} = \frac{1}{2}[1 + \mathrm{erf}(y^*)] \tag{29}$$

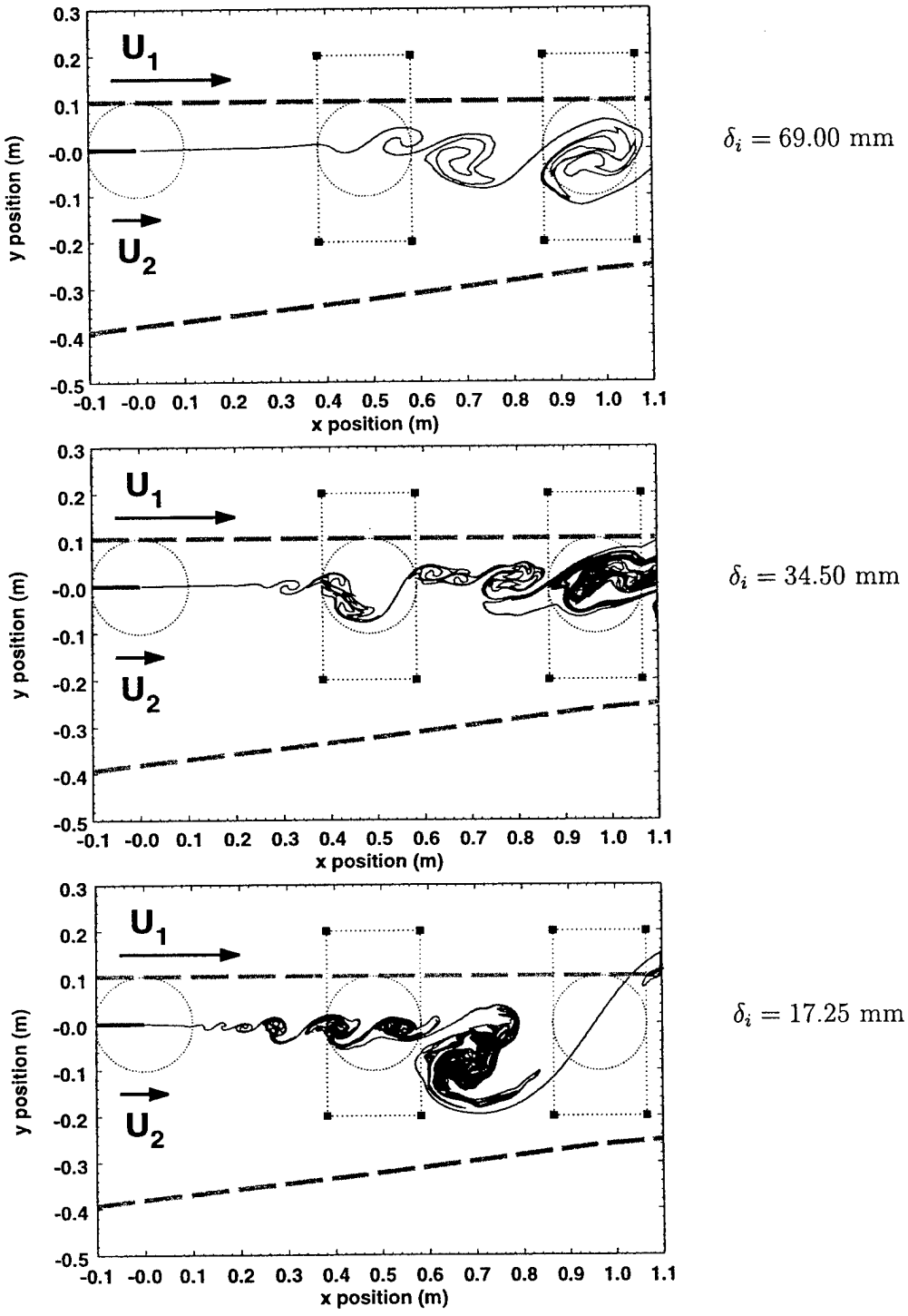

Figure 22. DVM shear layer rollup variation with initial thickness δ_i. Thick gray lines and circular windows illustrate vortex "roller" size relative to the AEDC test section. Smaller, dotted boxes show fields used in aero-optical computations.

and the $y-$position[80]

$$y^* = \frac{y - y_{0.5}}{\delta_\omega} \tag{30}$$

where $y_{0.5}$ is the $y-$position where $U = U_{cn}$. Using this nondimensionalization, the computed mean velocity profiles compare well with both incompressible and weakly compressible ($M_c = 0.51$) experimental measurements as shown in Fig. 23. DVM profiles are shown at several $x-$stations; the agreement increases with increasing x.

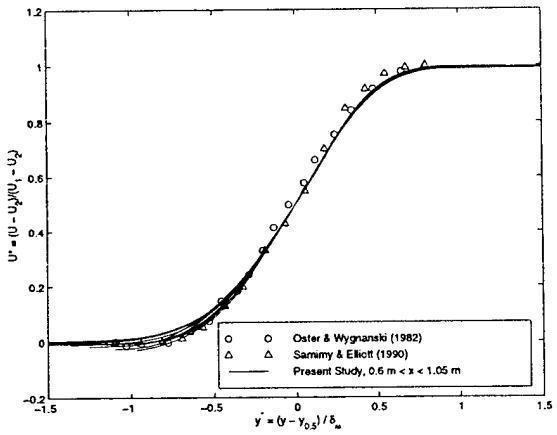

Figure 23. Comparison of DVM mean velocity profiles ($\delta_i/2 = 34.5$ mm) with experimental measurements in incompressible (Ref. 81) and weakly-compressible (Ref. 80) shear layers

Similarly, the *rms* streamwise and lateral velocity fluctuations as well as the Reynolds stress can be compared to the corresponding experimental results as shown in Figs. 24 and 25. In Figs. 24 and 25, the peak DVM values increase with increasing x. Similarity of the DVM velocity fluctuation and Reynolds stress profiles would be expected to occur at larger x than required for mean velocity profiles.[82] The variation in profile magnitude and shape with x suggests that similarity conditions have not yet been reached for the δ_i shown. Similarly-shaped longitudinal fluctuation profiles were obtained by Ashurst in a DVM[43] and in the water tunnel experiments of Browand

and his colleagues.[35,83] Winant and Browand's measurements showed, in fact, that the magnitude of the central peak increased with increasing x while the secondary peak (low-speed side "shoulder") gradually disappeared, taking on a shape normally associated with fully-turbulent shear layers.[35] Such a local maximum is predicted by Michalke's linear stability theory for spatially-growing shear layers[51] and suggests that the DVM behaves as if the splitter-plate boundary layers were laminar.

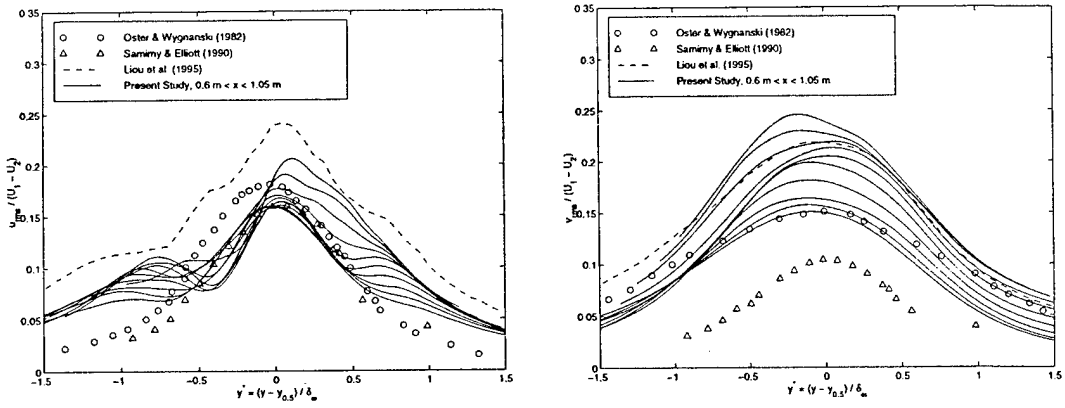

Figure 24. Comparison of DVM *rms* longitudinal (left) and lateral (right) velocity fluctuation profiles ($\delta_i/2 = 34.5$ mm) with experimental measurements in incompressible (Ref. 81) and weakly-compressible (Ref. 80) shear layers. A compressible-Euler numerical result is also shown (Ref. 84)

The growth of δ_ω with increasing x for our numerical simulation is shown in Fig. 26. The shear layer growth rate for all initial core sizes is the same. Once the shear layer's thickness, δ_ω, becomes large enough (versus vortex core size), the Kelvin-Helmholtz instability can be resolved and shear-layer roll-up begins. Upstream of this point (for a given initial vortex core diameter), the instability cannot be spatially resolved so $\delta_\omega \approx \delta_i$. According to the empirical literature,[39] the shear layer growth rate at the AEDC M_{c1} can be computed using Eq. 2 with $C_\delta = 0.085$ (and δ_ω in place of δ_{viz}). For the conditions used in our simulation ($r = 0.132$ and $s = 1$),

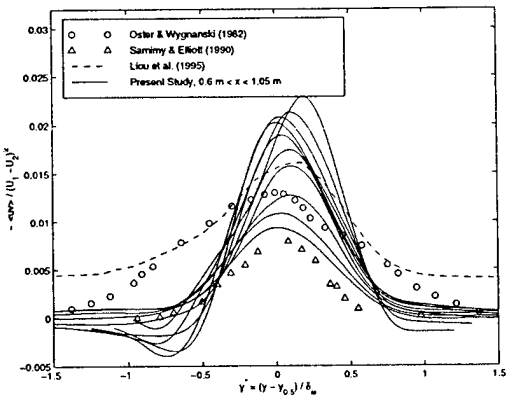

Figure 25. Comparison of DVM Reynolds stress profiles ($\delta_i/2 = 34.5$ mm) with experimental measurements in incompressible (Ref. 81) and weakly-compressible (Ref. 80) shear layers. A compressible-Euler numerical result is also shown (Ref. 84)

Eq. 28 would predict a growth rate of 0.130. The growth rate for the simulated shear layer, $\Delta\delta_\omega/(x - x_0) = 0.139$ (with $x_0 = 0.06$ m) is within 7% of this predicted value. As such, we felt the numerical simulation reasonably modeled the velocity field of a weakly-compressible shear layer.

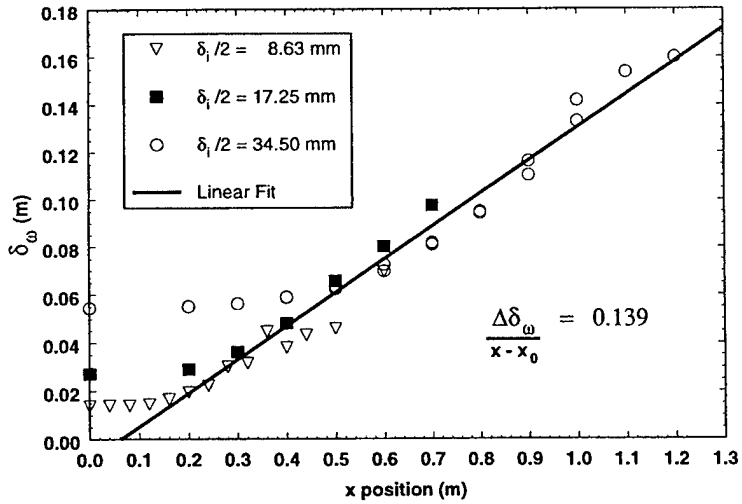

Figure 26. Growth of discrete vortex shear layer in terms of vorticity thickness.

REFERENCES

1. W. J. Smith, *Modern Optical Engineering: the Design of Optical Systems*, McGraw-Hill, New York, 1966.
2. G. W. Sutton, "Effects of turbulent fluctuations in an optically active fluid medium," *AIAA Journal* **7**(9), pp. 1737–1743, 1969.
3. V. I. Tatarski, *Wave Propagation in Turbulent Medium*, Dover, New York, 1961.
4. R. Tyson, *Principles of Adaptive Optics*, Academic Press, Inc., San Diego, 1991.
5. R. K. Tyson, "The status of astronomical adaptive optics systems," *O. E. Reports* **121**, pp. 11,13, Jan 1994.
6. R. J. Hugo and E. J. Jumper, "Experimental measurement of a time-varying optical path difference by the small-aperture beam technique," *Applied Optics* **35**, pp. 4436–4447, August 1996.
7. A. Verhoff, "Prediction of optical propagation losses through turbulent boundary/shear layers," in *Aero-Optical Phenomena*, K. G. Gilbert and L. J. Otten, eds., *Progress in Astronautics and Aeronautics Series* **80**, pp. 40–77, American Institute of Aeronautics and Astronautics, Inc., (New York), 1982.
8. H. W. Liepmann, "Deflection and diffusion of a light ray passing through a boundary layer," Report SM-14397, Douglas Aircraft Company, Santa Monica Division, Santa Monica, California, May 1952.
9. G. Havener, "Optical wave front variance: a study on analytic models in use today." AIAA Paper 92-0654, Jan 1992.
10. M. Malley, G. W. Sutton, and N. Kincheloe, "Beam-jitter measurements of turbulent aero-optical path differences," *Applied Optics* **31**, pp. 4440–4443, 1992.
11. H. H. Klein, M. M. Malley, O. Sapp, D. Shough, G. W. Sutton, and J. H.-Y. Yu, "Experimental measurements of the optical path difference of a four-meter

dual aerocurtain," in *Proceedings of the High Power Laser Optical components conference*, (Boulder, Colorado), Oct 1989.

12. D. Malacara, *Optical Shop Testing*, Wiley, New York, 1978.
13. E. J. Jumper and R. J. Hugo, "Quantification of aero-optical phase distortion using the small-aperture beam technique," *AIAA Journal* **33**(11), pp. 2151–2157, 1995.
14. E. J. Fitzgerald and E. J. Jumper, "Extension of the small-aperture beam technique to the measurement of full, 2-dimensional optical wavefronts," in *Optical Technology in Fluid, Thermal, and Combustion Flow*, S. S. Cha and J. D. Trollinger, eds., *SPIE - International Society of Optical Engineering* **3172**, 1997.
15. E. J. Fitzgerald and E. J. Jumper, "Two-dimensional, optical wavefront measurements using a small-aperture beam technique-derivative instrument," in *Proceedings of the International Conference on Optical Technology and Image Processing in Fluid, Thermal, and Combustion Flow, (VSJ-SPIE 98)*, Dec 1998.
16. J. M. Cicchiello and E. J. Jumper, "Far-field optical degradation due to near-field transmission through a turbulent heated jet," *Applied Optics* **36**, pp. 6441–6452, Sep 1997.
17. R. J. Hugo, E. J. Jumper, G. Havener, and C. Stepanek, "Time-resolved aero-optical measurements of a wavefront aberrated by a compressible free shear layer." AIAA Paper 95-1979, Jun 1995.
18. R. J. Hugo, E. J. Jumper, G. Havener, and C. Stepanek, "Time-resolved wave front measurements through a compressible free shear layer," *AIAA Journal* **35**(4), pp. 671–677, 1997.
19. E. J. Fitzgerald and E. J. Jumper, "Optical propagation through compressible shear layers." Presented by: D. T. Kyrazis, 2nd Annual Directed Energy Symposium, November 1999.

20. D. T. Kyrazis. Personal communication, 5 Nov 1999.

21. E. J. Jumper, "Recent advances in the measurement and analysis of dynamic aero-optic interactions (review paper)." AIAA Paper 97-2350, Jun 1997.

22. R. J. Hugo, *Quantifying the Spatio-Temporal Effects of Optically-Active Turbulent Flowfields on a Coherent Optical Wave.* PhD thesis, University of Notre Dame, Notre Dame, Indiana, Apr 1995.

23. P. E. Cassady, S. F. Birch, and P. J. Terry, "Aero-optical analysis of compressible flow over an open cavity," *AIAA Journal* **27**(6), pp. 758–762, 1989.

24. N. D. Sandham and W. C. Reynolds, "Compressible mixing layer: Linear theory and direct simulation," *AIAA Journal* **28**(4), pp. 618–624, 1990.

25. N. D. Sandham and W. C. Reynolds, "Three-dimensional simulations of large eddies in the compressible mixing layer," *Journal of Fluid Mechanics* **224**, pp. 133–158, 1991.

26. P. E. Dimotakis, H. J. Catrakis, and D. C. L. Fourguette, "Beam propagation and wavefront-phase integrals in high reynolds number shear layers and jets." AIAA Paper 98-2833, Jun 1998.

27. P. E. Dimotakis. Personal communication, 17 Jun 1998.

28. D. Papamoschou. Personal communication, 17 Jun 1998.

29. G. W. Sutton. Personal communication, 17 Jun 1998.

30. E. J. Fitzgerald and E. J. Jumper, "Aperture effects on the aero-optical distortions measured for a compressible shear layer." AIAA Paper 2000-0991, Jan 2000.

31. E. J. Fitzgerald, *The Shear Layer Compressility Mechanism and Its Role in Creating Aero-Optical Distortions.* PhD thesis, University of Notre Dame, Notre Dame, Indiana, Apr 2000. (In review).

32. E. J. Fitzgerald and E. J. Jumper, "Aperture effects on the aero-optical distortions produced by a compressible shear layer," *AIAA Journal* , 2000. (In Review).

33. G. Havener and F. Heltsley, "Design aspects and preliminary holographic-PIV measurements for a subsonic free shear layer flow channel." AIAA Paper 94-2550, Jun 1994.

34. G. L. Brown and A. Roshko, "On density effects and large structure in turbulent mixing layers," *Journal of Fluid Mechanics* **64**(4), pp. 775–816, 1974.

35. C. D. Winant and F. K. Browand, "Vortex pairing: The mechanism of turbulent mixing-layer growth at moderate Reynolds number," *Journal of Fluid Mechanics* **63**(2), pp. 237–255, 1974.

36. P. E. Dimotakis and G. L. Brown, "The mixing layer at high reynolds number: Large structure dynamics and entrainment," *Journal of Fluid Mechanics* **78**, pp. 535–560, 1976.

37. J. L. Hall, P. E. Dimotakis, and H. Rosemann, "Experiments in nonreacting compressible shear layers," *AIAA Journal* **31**(12), pp. 2247–2254, 1993.

38. D. Papamoschou and A. Roshko, "Observations of supersonic free shear layers." AIAA Paper 86-0162, Jan 1986.

39. D. Papamoschou and A. Roshko, "The compressible turbulent layer: An experimental study," *Journal of Fluid Mechanics* **197**, pp. 453–477, 1988.

40. E. J. Fitzgerald and E. J. Jumper, "Further consideration of compressibility effects on shear-layer optical distortion." AIAA Paper 99-3617, Jun 1999.

41. F. O. Thomas, "Structure of mixing layers and jets," *Applied Mechanics Review* **44**, pp. 119–153, 1991.

42. Y. P. Tsai and W. H. Christiansen, "Two-dimensional numerical simulation of shear-layer optics," *AIAA Journal* **28**(12), pp. 2092–2097, 1990.

43. W. T. Ashurst, "Numerical simulation of turbulent mixing layers via vortex dynamics," in *Turbulent Shear Flows I*, F. Durst *et al.*, ed., pp. 402–413, Springer-Verlag, (Berlin), 1979.

44. O. Inoue, "Vortex simulation of a turbulent mixing layer," *AIAA Journal* **23**(3), pp. 367–373, 1985.

45. A. F. Ghoniem, "Vortex simulation of reacting shear flow," in *Numerical Approaches to Combustion Modeling*, E. S. Oran and J. P. Boris, eds., *Progress in Astronautics and Aeronautics Series* **135**, pp. 305–348, American Institute of Aeronautics and Astronautics, Inc., (New York), 1990.

46. A. J. Smits and J.-P. Dussauge, *Turbulent Shear Layers in Supersonic Flow*, American Institute of Physics, Woodbury, New York, 1996.

47. M. V. Morkovin, "Effects of compressibility on turbulent flows," in *Mécanique de la Turbulence*, A. Favre, ed., pp. 367–380, CNRS, (Paris), 1962.

48. K. G. Gilbert, "KC-135 aero-optical boundary-layer/shear-layer experiments," in *Aero-Optical Phenomena*, K. G. Gilbert and L. J. Otten, eds., *Progress in Astronautics and Aeronautics Series* **80**, pp. 306–324, American Institute of Aeronautics and Astronautics, Inc., (New York), 1982.

49. R. J. Hugo and E. J. Jumper, "Constant current anemometry and its impact on aero-optical measurements." AIAA Paper 95-1986, Jun 1995.

50. R. J. Hugo and E. J. Jumper, "Implications of the homogeneous turbulence assumption on the aero-optic linking equation," in *Optical Techniques in Fluid, Thermal, and Combustion Flow*, S. S. Cha and J. D. Trollinger, eds., *SPIE - International Society of Optical Engineering* **2546**, pp. 189–200, 1995.

51. A. Michalke, "On spatially growing disturbances in an inviscid shear layer," *Journal of Fluid Mechanics* **23**, pp. 521–544, 1965.

52. P. A. Monkewitz and P. Huerre, "The influence of the velocity ratio on the spatial instability of mixing layers," *Physics of Fluids* **25**, pp. 1137–1143, 1983.

53. C. M. Ho and L. S. Huang, "Subharmonics and vortex merging in mixing layers," *Journal of Fluid Mechanics* **119**, pp. 443–473, 1982.

54. C. M. Ho and P. Huerre, "Perturbed free shear layers," in *Annual Review of Fluid Mechanics*, J. L. Lumley, M. V. Dyke, and J. V. Wehausen, eds., vol. 16, pp. 365–424, Annual Reviews Inc., (Palo Alto, California), 1984.

55. T. C. Corke and D. A. Cavalieri, "Controlled experiments on instabilities and transition to turbulence in supersonic boundary layers." AIAA Paper 97-1817, Jun 1997.

56. T. C. Corke, D. A. Cavalieri, and E. Matlis, "Boundary layer instability on a sharp cone at Mach 3.5 with controlled input," *AIAA Journal* , 1999. (In Review).

57. R. J. Hugo and E. J. Jumper, "Experimental measurement of a time-varying optical path difference using the small-aperture beam technique," in *Optical Diagnostics in Fluid and Thermal Flow*, S. S. Cha and J. D. Trollinger, eds., *SPIE - International Society of Optical Engineering* **2005**, pp. 116–128, 1993.

58. E. J. Fitzgerald and E. J. Jumper, "Shear layer optical distortions due to compressibility vs. passive scalars." AIAA Paper 98-2834, Jun 1998.

59. R. J. Hugo and E. J. Jumper, "Applicability of the aero-optic linking equation to a highly-coherent, transitional shear layer," *Applied Optics* , 2000. (To be published).

60. E. J. Fitzgerald and E. J. Jumper, "Two-dimensional, optical wavefront measurements using a small-aperture beam technique-derivative instrument," *Optical Engineering* , 2000. (In Review).

61. H. A. Stine and W. Winovich, "Light diffusion through high-speed turbulent boundary layers," Research Memorandum A56B21, NACA, Washington, May 1956.

62. L. L. Baskins and Hamilton, "Preliminary wind tunnel investigation on the optical transmission characteristics of a supersonic turbulent boundary layer," Report G.M.-1.27, Northrop Aircraft Company, April 1952.

63. L. L. Baskins and Hamilton, "The effect of boundary layer thickness upon the optical transmission characteristics of a supersonic turbulent boundary layer," Report NAI-54-756, Northrop Aircraft Company, Nov 1954.

64. H. G. Booker and W. E. Gordon, "A theory of radio scattering in the troposphere," in *Proceedings of the I.R.E.*, vol. 38, pp. 401–412, April 1950.

65. R. Villars and V. F. Weisskopf, "The scattering of electromagnetic waves by turbulent atmospheric fluctuations," *Physical Review* **94**, pp. 232–240, Apr 1954.

66. G. W. Sutton, "Aero-optical foundations and applications," *AIAA Journal* **23**, pp. 1525–1537, Oct 1985.

67. K. G. Gilbert and L. J. Otten, eds., *Aero-Optical Phenomena*, vol. 80 of *Progress in Astronautics and Aeronautics Series*, American Institute of Aeronautics and Astronautics, Inc., New York, 1982.

68. J. D. Trollinger, "Aero-optical characterization of aircraft optical turrets by holography, interferometry and shadowgraph," in *Aero-Optical Phenomena*, K. G. Gilbert and L. J. Otten, eds., *Progress in Astronautics and Aeronautics Series* **80**, pp. 200–217, American Institute of Aeronautics and Astronautics, Inc., (New York), 1982.

69. W. C. Rose and D. A. Johnson, "Unsteady density and velocity measurements in the 6 x 6 ft wind tunnel," in *Aero-Optical Phenomena*, K. G. Gilbert and L. J.

Otten, eds., *Progress in Astronautics and Aeronautics Series* **80**, pp. 218–232, American Institute of Aeronautics and Astronautics, Inc., (New York), 1982.

70. D. Kelsall, "Rapid interferometric technique for MTF measurements in visible or infrared region," *Applied Optics* **12**, pp. 1398–1399, 1973.
71. M. V. Klein, *Optics*, John Wiley and Sons, New York, 1970.
72. R. L. Panton, *Incompressible Flow*, John Wiley & Sons, New York, 1984.
73. S. K. Lele, "Compressibility effects on turbulence," in *Annual Review of Fluid Mechanics*, J. L. Lumley, M. V. Dyke, and H. L. Reed, eds., vol. 26, pp. 211–254, Annual Reviews Inc., (Palo Alto, California), 1994.
74. L. J. Leep, J. C. Dutton, and R. F. Burr, "Three-dimensional simulations of compressible mixing layers: Visualizations and statistical analysis," *AIAA Journal* **31**(11), pp. 2039–2046, 1993.
75. L. Rosenhead, "The formation of vortices from a surface discontinuity," *Proceedings of the Royal Society - Series A* **134**, pp. 170–192, 1932.
76. A. J. Chorin and P. S. Bernard, "Discretization of a vortex sheet, with an example of roll-up," *Journal of Computational Physics* **13**, pp. 423–429, 1973.
77. J. T. Beale and A. Majda, "High order accurate vortex methods with explicit velocity kernels," *Journal of Computational Physics* **58**, pp. 188–208, 1985.
78. A. F. Ghoniem, G. Heidarinejad, and A. Krishnan, "Numerical simulation of a thermally stratified shear layer using the vortex element method," *Journal of Computational Physics* **79**, pp. 135–166, 1988.
79. H. Schlichting, *Boundary-Layer Theory*, McGraw-Hill, New York, seventh ed., 1979.
80. M. Samimy and G. S. Elliott, "Effects of compressibility on the characteristics of free shear layers," *AIAA Journal* **28**(3), pp. 439–445, 1990.

81. I. Wygnanski and D. Oster, "The forced mixing layer between parallel streams," *Journal of Fluid Mechanics* **123**, pp. 91–130, 1982.

82. F. M. White, *Viscous Fluid Flow*, McGraw-Hill, New York, second ed., 1991.

83. F. K. Browand and P. D. Weidman, "Large scales in the developing mixing-layer," *Journal of Fluid Mechanics* **76**, pp. 127–144, 1976.

84. T. Liou, W. Lien, and P. Hwang, "Compressibility effects and mixing enhancement in turbulent free shear flows," *AIAA Journal* **33**(12), pp. 2332–2338, 1995.